

Ultraviolet background fluctuations with clustered sources

Vincent Desjacques^{*}, Azadeh Moradinezhad Dizgah and Matteo Biagetti

*Département de Physique Théorique and Center for Astroparticle Physics (CAP), Université de Genève,
24 quai Ernest Ansermet, CH-1211 Genève, Switzerland*

ABSTRACT

We develop a count-in-cells approach to the distribution of ultraviolet background fluctuations that includes source clustering. We demonstrate that an exact expression can be obtained if the clustering of ionizing sources follows the hierarchical ansatz. In this case, the intensity distribution depends solely on their 2-point correlation function. We show that the void scaling function of high redshift mock quasars is consistent with the Negative Binomial form, before applying our formalism to the description of HeII-ionizing fluctuations at the end of helium reionization. The model inputs are the observed quasar luminosity function and 2-point correlation at $z \sim 3$. We find that, for an (comoving) attenuation length $\lesssim 55$ Mpc, quasar clustering contributes less than 30% of the variance of intensity fluctuations so long as the quasar correlation length does not exceed ~ 15 Mpc. We investigate also the dependence of the intensity distribution on the large-scale environment. Differences in the mean HeII-ionizing intensity between low- and high-density regions could be a factor of few if the sources are highly clustered. An accurate description of quasar demographics and their correlation with strong absorption systems is required to make more precise predictions.

Key words: cosmology: theory, reionization, intergalactic medium, quasars: general

1 INTRODUCTION

Modelling helium reionization is challenging because of the wide dynamical range that must be achieved to account simultaneously for the scarcity and clustering of the sources (quasars) and the physical properties of the low density intergalactic medium (IGM). Therefore, a number of hybrid methods combining analytic approaches with numerical simulations have been developed to address this problem (e.g. Sokasian, Abel & Hernquist 2002; Gleser et al. 2005; Bolton et al. 2006; Paschos et al. 2007; Furlanetto & Oh 2008; Faucher-Giguère et al. 2009; Meiksin & Tittley 2012). Nevertheless, several issues, including the contribution of quasar clustering to the variance of the helium-ionizing fluctuations towards the end of HeII reionization ($z \sim 3$), are still being debated. Whereas variations in the HI-ionizing background are expected to be small owing to the large (comoving) attenuation length (or mean free path) of hydrogen-ionizing photons, $r_0 \sim 200$ Mpc (Prochaska et al. 2014), recent studies indicate that $r_0 \sim 30 - 50$ Mpc only for helium-ionizing photons around $z \sim 3$ (Bolton et al. 2006; Furlanetto & Oh 2008; Davies & Furlanetto 2014). This is not much larger than the observed clustering length $r_\xi \gtrsim$

15–30 Mpc of bright quasars in the same redshift range (e.g. Shen et al. 2007; Francke et al. 2008). Clearly, $r_\xi/r_0 \gtrsim 1$ is a necessary condition for source clustering to be important. However, the abundance of sources furnishes another characteristic length: the average source separation $l = \bar{n}^{-1/3}$. Hence, the condition $r_0/l \gg 1$ or, equivalently, a large number of sources per attenuation volume so that Poisson fluctuations are small relative to clustering effects, must also be satisfied. While bright quasars are very rare and, therefore, certainly do not meet this criterion, faint quasars are much more abundant, though possibly not as strongly clustered as their bright companions. These considerations show that the importance of source clustering at the end of HeII reionization may strongly depend on the assumed quasar properties.

Recently, Dixon, Furlanetto & Mesinger (2014) have addressed the impact of quasar clustering using a semi-numeric method, in which dark matter haloes are identified in realisations of the linear density field using the excursion set approach. They have found a relatively weak effect. However, given the current uncertainties on the demographics of high redshift quasars, it would be desirable to revisit this issue and explore a wider spectrum of quasar clustering amplitudes.

^{*} E-mail: Vincent.Desjacques@unige.ch

In this paper, we will investigate this issue analytically

using an approach based on the count-in-cells formalism (see e.g. Fall et al. 1976; White 1979; Peebles 1980; Fry 1986; Balian & Schaeffer 1989; Szapudi & Colombi 1996). Our model generalizes to clustered sources the early work of Zuo (1992); Fardal & Shull (1993); Meiksin & White (2003), who considered the probability distribution of ionizing intensity induced by randomly distributed sources. The assumption of hierarchical ansatz is a crucial ingredient of our method. It is efficient only if the source distribution follows the hierarchical scaling. We will show that this is the case of mock quasars at high redshift. This will enable us to explore very different quasar clustering configurations, at the expenses of a detailed modelling of the small-scale IGM physics.

This paper is organized as follows. In Sec.2, we introduce our count-in-cell approach, discuss the validity of the hierarchical ansatz for high redshift quasars and demonstrate that the intensity distribution $P(J)$ can be worked out exactly (within the simplifications of such analytic approaches) if the sources follows the hierarchical scaling. In Sec.3, we derive explicit scaling solutions for the low- and high-intensity tails and briefly discuss the numerical implementation of our result. In Sec.4, we apply our method to the distribution of HeII-ionizing intensity at the completion of helium reionization. We discuss our results in Sec.5 and conclude in Sec.6. We shall hereafter use $h = 0.7$ in all unit conversions.

2 THEORETICAL CONSIDERATIONS

The distribution of ionizing intensities $P(J)$ has been worked out by Zuo (1992); Fardal & Shull (1993); Meiksin & White (2003) for Poisson distributed sources. Here, we extend their calculation to clustered sources. We begin with the introduction of position-dependent weights into the count-in-cells formalism before demonstrating that, if the sources follow the hierarchical scaling, then $P(J)$ can be recast into a simple expression.

2.1 Cell counts with position-dependent weight

Following White (1979), we define the probability to have a cell of volume V empty of particles except at positions $\mathbf{x}_1, \dots, \mathbf{x}_N$ as

$$P\{X_1 \dots X_N | \Phi_0(V)\} = P\{X_1 \dots X_N | \Phi_0(V)\} e^{\mathcal{W}_0(V)}. \quad (1)$$

The probability $P_0 \equiv P(\Phi_0(V))$ to have an empty cell is the exponential of the conditional void correlation (Fall et al. 1976; White 1979; Fry 1985)

$$\begin{aligned} \mathcal{W}_0(V) &= \sum_{k=1}^{\infty} \frac{(-\bar{n})^k}{k!} \int_V d^3\mathbf{x}_1 \dots \int_V d^3\mathbf{x}_k \xi_k(\mathbf{x}_1, \dots, \mathbf{x}_k) \quad (2) \\ &= \sum_{k=1}^{\infty} \frac{(-\bar{N})^k}{k!} \bar{\xi}_k(V). \end{aligned}$$

Here, \bar{n} is the average number density of objects, $\bar{N} = \bar{n}V$, $\xi_k(\mathbf{x}_1, \dots, \mathbf{x}_k)$ is the k -point irreducible correlation function and

$$\bar{\xi}_k(V) \equiv \frac{1}{V^k} \int_V d^3\mathbf{x}_1 \dots \int_V d^3\mathbf{x}_k \xi_k(\mathbf{x}_1, \dots, \mathbf{x}_k) \quad (3)$$

is its volume-average. Eq.(2) assumes that the volume can be split into many small subvolumes, such that each individual cell is either empty or contains exactly one object. It would not hold if several objects could have the same location. Note also that $\xi_1(\mathbf{x}) \equiv 1$ for a homogeneous process. We will relax this assumption in Sec.4.3.

The void probability function P_0 is a generating function for the count-in-cells probabilities. Namely, the probability to have exactly N objects in (randomly-located) cells of volume V is

$$P_N(V) = \frac{(-\bar{n})^N}{N!} \frac{d^N}{d\bar{n}^N} \exp[\mathcal{W}_0(V)], \quad (4)$$

where the derivatives are evaluated at constant $\bar{\xi}_k$ (White 1979; Sheth 1996). The positive definite, normalized probabilities $P_N(V)$ impose strong constraints on the behaviour of \mathcal{W}_0 as a function of V or, equivalently, \bar{N} (e.g. Fry 1985; Balian & Schaeffer 1989). Clearly, we must have $\mathcal{W}_0(\bar{N}) \leq 0$. Furthermore, the conditions $P_1 > 0$ and $P_2 > 0$ require

$$\frac{\partial \mathcal{W}_0}{\partial \bar{N}} > 0 \quad \text{and} \quad \frac{\partial^2 \mathcal{W}_0}{\partial \bar{N}^2} + \left(\frac{\partial \mathcal{W}_0}{\partial \bar{N}} \right)^2 > 0. \quad (5)$$

Assuming that the conditional void probability is locally of the form $\mathcal{W}_0(\bar{N}) = -\bar{N}^\beta$, this translates into the bound $0 < \beta < 1$. Finally, since we must recover the Poisson regime $\mathcal{W}_0(\bar{N}) = -\bar{N}$ in the limit $\bar{N} \rightarrow 0$, this implies that $\mathcal{W}_0(\bar{N})$ is a convex, monotonically decreasing function of \bar{N} that satisfies $-\bar{N} \leq \mathcal{W}_0(\bar{N}) < 0$. In other words, P_0 is smallest for a Poisson process.

For the purpose of modelling $P(J)$, we are interested in computing the probability distribution $P_\omega(V)$ defined as

$$\begin{aligned} P_\omega(V) &= \sum_{N=0}^{\infty} \frac{1}{N!} \int \dots \int P\{X_1 \dots X_N | \Phi_0(V)\} \quad (6) \\ &\quad \times \omega(\mathbf{x}_1) \dots \omega(\mathbf{x}_N) e^{\mathcal{W}_0(V)}, \end{aligned}$$

where $\omega(\mathbf{x})$ is a position-dependent weight and the multiplicative factor of $1/N!$ reflects the fact that the objects are identical. Details of the calculation can be found in Appendix §A. In short, substituting the explicit expression of $P\{X_1 \dots X_N | \Phi_0(V)\}$, which involves products of the conditional correlation functions \mathcal{W}_N , collecting the terms of same order in \bar{n} shows that the series expansion Eq.(6) nicely re-sums into the compact expression

$$P_\omega(V) = e^{\mathcal{W}_\omega(V)} - e^{\mathcal{W}_0(V)}. \quad (7)$$

The probability $P_0 = \exp(\mathcal{W}_0)$ of an empty cell is subtracted because it does not carry any weight. Furthermore, in analogy with (minus) the conditional void correlation $\mathcal{W}_0(V)$, we have defined

$$\begin{aligned} \mathcal{W}_\omega(V) &= \sum_{k=1}^{\infty} \frac{(-\bar{n})^k}{k!} \int_V d^3\mathbf{x}_1 \dots \int_V d^3\mathbf{x}_k \xi_k(\mathbf{x}_1, \dots, \mathbf{x}_k) \\ &\quad \times (1 - \omega(\mathbf{x}_1)) \dots (1 - \omega(\mathbf{x}_k)). \quad (8) \end{aligned}$$

Note the similarity of this expression with the partition function $Z[J]$ introduced by Szapudi & Szalay (1993). Eq.(8) indeed is their $Z[J]$ with a source term $J(\mathbf{x}) = \omega(\mathbf{x}) - 1$.

2.2 Application to the UV ionizing background

The characterization of fluctuations in the ionizing background generated by clustered sources provides an inter-

esting application for our weighted probability distribution $P_\omega(V)$.

Namely, let $\{\mathbf{x}_k\}$, $k = 1, \dots, N$, be the comoving positions of N quasars distributed inside a cell of volume $V \propto R^3$ at redshift z . Each of them emits ionizing radiation, so that the angle-averaged specific intensity of ionizing photons (in units of $\text{ergs s}^{-1} \text{cm}^{-2} \text{sr}^{-1}$) at the center of the cell is

$$J_k(\mathbf{x}_k) = (1+z)^2 \frac{L_k}{(4\pi r_k)^2} e^{-r_k/r_0}. \quad (9)$$

$r_k = |\mathbf{x}_k|$ is the modulus of the separation vector, L_k is the quasar luminosity (in ergs s^{-1}) and r_0 is the attenuation length of ionizing photons in the intergalactic medium. We will hereafter ignore the multiplicative factor of $(1+z)^2$ and quote specific intensities relative to their mean. This factor should, of course, be re-introduced in order to compute the absolute photoionization rate Γ etc.

The probability to have an angle-averaged specific intensity J at the center of the cell is obtained upon summing over all the configurations subject to the constraint $\sum_k J_k = J$. In other words, each configuration of N sources contributes a factor of

$$\int d\alpha_1 \dots d\alpha_N \phi(\alpha_1) \dots \phi(\alpha_N) \times P\{X_1 \dots X_N \Phi_0(V)\} \times \delta_D(J_1 + \dots + J_N - J) \quad (10)$$

to the total probability. The measure $\phi(\alpha)d\alpha$ with $\alpha = L/L^*$ is the probability density for the quasar luminosity, $L^* = L^*(z)$ is a characteristic, usually redshift-dependent luminosity and the specific intensity J_k now reads $J_k = \alpha_k L^* \exp(-r_k/r_0)/(4\pi r_k)^2$. We will henceforth assume that the reduced correlations $\bar{\xi}_k$ do not depend on α , yet our results can be straightforwardly extended to include a dependence of clustering on α .

Substituting the Laplace representation of the Dirac delta in Eq.(10),

$$\delta_D(J_1 + \dots + J_N - J) = \frac{1}{2\pi i} \int_{-i\infty}^{+i\infty} ds e^{s(J - J_1 - \dots - J_N)}, \quad (11)$$

integrating the variables $\mathbf{x}_1, \dots, \mathbf{x}_N$ and summing over $N \geq 0$, we find that the probability $P(J)$ to have a total specific intensity J at the center of a cell of volume V is exactly given by Eq.(6) with a weight

$$\omega(\mathbf{x}_k) = \Theta_H(R - |\mathbf{x}_k|) \int_{\alpha_{\min}}^{\alpha_{\max}} d\alpha_k \phi(\alpha_k) e^{-sJ_k(\mathbf{x}_k)} \quad (12)$$

assigned to each object. The Heaviside function $\Theta_H(R - |\mathbf{x}|)$ delimits the cell boundaries, while the lower and upper limits of the integral are $\alpha_{\min} = L_{\min}/L^*$, $\alpha_{\max} = L_{\max}/L^*$. Finally, s is the variable conjugate to J . Therefore, $P(J)$ takes the compact form

$$P(J) = \frac{1}{2\pi i} \int_{-i\infty}^{+i\infty} ds e^{sJ + \mathcal{W}_\omega(V)}, \quad (13)$$

where the weight ω is given by Eq.(12). The contribution from the void conditional probability can be ignored since it is independent of s and, therefore, only contributes at $J = 0$ (empty cells do not generate any radiation). In other words, $P(J)$ truly is the distribution of intensity conditioned on the cell being not empty. It is, of course, normalized to unity.

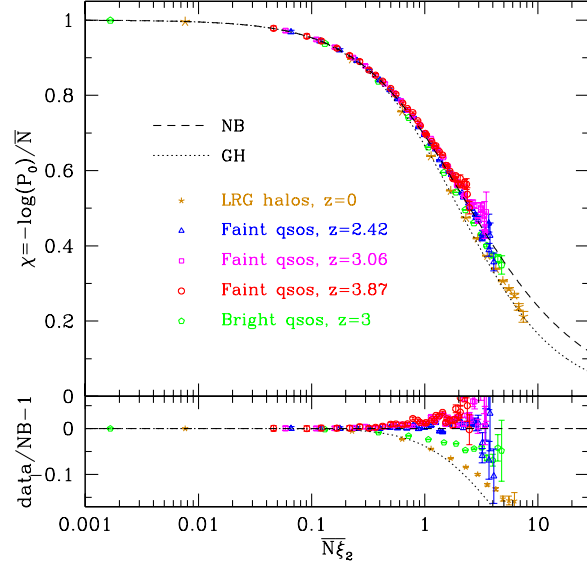


Figure 1. *Top panel* : Void scaling function χ as a function of average clustering strength $\bar{N}\bar{\xi}_2$. (Orange) stars represent χ for $z = 0$ haloes. (Blue) triangles, (magenta) squares and (red) circles indicate the scaling for the mock quasars of the “faint” sample at $z = 2.4, 3$ and 3.9 , respectively. (Green) pentagons are χ for the “bright” sample at $z = 3$ (see text). The dashed and dotted curves indicate the void scaling in the Negative Binomial (NB) and Geometric Hierarchical (GH) models, respectively. *Bottom panel* : Fractional deviation from the NB scaling (color online).

As we will see shortly, the Laplace transform yields a more intuitive description than the Fourier transform. In practice however, the Fourier representation of the Dirac delta turns out to be more convenient for the numerical evaluation of $P(J)$:

$$P(J) = \frac{1}{2\pi} \int_{-\infty}^{+\infty} ds e^{-isJ + \mathcal{W}_\omega(V)}, \quad (14)$$

with the weight given by

$$\omega(\mathbf{x}_k) = \Theta_H(R - |\mathbf{x}_k|) \int_{\alpha_{\min}}^{\alpha_{\max}} d\alpha_k \phi(\alpha_k) e^{isJ_k(\mathbf{x}_k)} \quad (15)$$

The numerical implementation will be discussed in more detail in §3.3.

2.3 Specialisation to hierarchical models

The evaluation of Eqs.(13) or (14) is not a trivial task since it requires knowledge of all reduced correlation functions ξ_k of the sources. Interestingly however, $P(J)$ can be easily computed when the clustering of sources follow the hierarchical ansatz. In this case, all the information about source clustering is contained in the 2-point correlation function and the void scaling function.

2.3.1 Hierarchical scaling and random dilutions

In the hierarchical approximation, volume-averaged correlation functions are of the form $\bar{\xi}_k = S_k \bar{\xi}_2^{k-1}$ where the coefficients S_k (which are ratios of connected moments) are generally scale-independent, and converge towards $S_k = k^{k-2}$

in the rare halo limit (Bernardeau & Schaeffer 1999). Hence, we can recast the logarithm of the void probability into the series (Fry 1986)

$$\begin{aligned} \mathcal{W}_0(V) &= -\bar{N} \sum_{k=1}^{\infty} \frac{(-1)^{k-1}}{k!} S_k (\bar{N} \bar{\xi}_2)^{k-1} \\ &\equiv -\bar{N} \chi(\bar{N} \bar{\xi}_2). \end{aligned} \quad (16)$$

Consequently, the void scaling function

$$\chi = -\frac{\ln(P_0)}{\bar{N}} = -\frac{\mathcal{W}_0(V)}{\bar{N}} \quad (17)$$

depends on the distance r through $\bar{\xi}_2(r)$ only. Note that we recover $\chi \equiv 1$ for a pure Poisson distribution $P_0 = e^{-\bar{N}}$, whereas $0 < \chi < 1$ holds for any clustered distribution.

Even though observational data (Bouchet et al. 1993; Gaztanaga 1994; Croton et al. 2004; Ross, Brunner & Myers 2006) and numerical simulations (Fry et al. 2011) indicate that the hierarchical amplitudes S_k of the galaxy distribution depend on scale, the simulated and observed void probabilities appear to obey the hierarchical scaling Eq.(16). As shown by Fry & Colombi (2013), this can be explained by the halo model if the distribution of host haloes follows the hierarchical pattern. Moreover, one should expect that different populations of tracers are described by different void scaling relations.

Several analytic formulae have been proposed for the void scaling function (see Fry 1986, for a discussion). Comparison with N-body simulations indicate that the geometric hierarchical (GH, e.g. Carruthers & Shih 1983) and negative binomial (NB, e.g. Hamilton 1988) models are good approximation for galaxies (subhaloes) and haloes extracted from N-body simulations, respectively (Fry & Colombi 2013). The corresponding functional form of χ is

$$\chi(\bar{N} \bar{\xi}_2) = \frac{\ln(1 + \bar{N} \bar{\xi}_2)}{\bar{N} \bar{\xi}_2} \quad (\text{NB}) \quad (18)$$

$$\chi(\bar{N} \bar{\xi}_2) = \frac{1}{1 + \frac{1}{2} \bar{N} \bar{\xi}_2} \quad (\text{GH}) \quad (19)$$

Clustering becomes significant in the regime $\bar{N} \bar{\xi}_2 \gtrsim 1$, i.e. high number densities and/or large correlation length.

Random dilutions of a point distribution will affect the average number density \bar{N} but not the correlation functions $\bar{\xi}_k$ (Peebles 1980; Lahav & Saslaw 1992; Sheth 1996). However, while the void scaling functions of the parent and diluted sample generally differ, some distributions preserve their functional form. As shown in Sheth (1996), this is the case of the NB model. This can easily be seen upon rewriting the generating functional $g(\lambda) = \sum_N P_N \lambda^N$ as

$$g(\lambda) = [1 + \bar{N} \bar{\xi}_2 (1 - \lambda)]^{-1/\bar{\xi}_2}. \quad (20)$$

Since a random dilution is equivalent to the transformation $\lambda \rightarrow p\lambda + q$, where $p < 1$ is the dilution factor and $q = 1 - p$ (Lahav & Saslaw 1992), we find

$$g(p\lambda + q) = [1 + p\bar{N} \bar{\xi}_2 (1 - \lambda)]^{-1/\bar{\xi}_2}, \quad (21)$$

which shows that the diluted distribution follows the NB scaling with a number density $p\bar{N}$ (Sheth 1996).

2.3.2 Quasar void scaling function

For HeII-reionization discussed in Sec. §4, quasars are the relevant ionizing sources.

In order to ascertain whether the void scaling function of quasars also follows the hierarchical scaling without going into a detailed modelling of their distribution, we use the synthetic quasar catalogues of Croton (2009) extracted from the MILLENNIUM simulation (Springel et al. 2005). These catalogues were constructed by abundance matching under the assumption that quasars populate both parent haloes and subhaloes above the minimum resolved halo mass, i.e. $M_{\min} \sim 10^{11} M_{\odot}/h$. Quasars are thus randomly sub-sampling (sub)haloe centres of mass $M > M_{\min}$ with a dilution factor p equal to their duty cycle $f = t_Q/t_H$. Here, t_Q and t_H are the typical quasar lifetime and the Hubble time at redshift z , respectively (Martini & Weinberg 2001; Haiman & Hui 2001). We adopt a duty cycle of $f \approx 0.037$, which leads to a quasar number density of $\bar{n} \approx 6.0 \times 10^{-4} h^3 \text{Mpc}^{-3}$ at $z = 3$. We consider three samples at $z = 2.42, 3.06$ and 3.87 , which we refer to as the “faint” quasars since they include (sub)haloes down to a relatively small mass.

Since quasar demographics are relatively uncertain, we generate an additional mock catalogue. We assume that quasars populate only parent haloes above the minimum mass, although small-scale clustering measurements indicate that a halo may host more than one shining quasar simultaneously (Hennawi et al. 2006; Myers et al. 2008; Padmanabhan et al. 2009). This should be a reasonable assumption at high redshift and for separations $r \gtrsim 1 h^{-1} \text{Mpc}$ larger than the typical halo scale (Conroy & White 2013). We use dark matter haloes extracted from N-body simulations evolving 1024^3 particles in periodic boxes of size $1500 h^{-1} \text{Mpc}$ (for details about the simulations, see Biagetti et al. 2014). We sample all haloes above the minimum resolved halo mass, i.e. $M_{\min} = 5 \times 10^{12} M_{\odot}/h$ and $p = 1$. We will refer to this sample as the “bright” quasars since they only trace massive haloes. We focus on the snapshot at $z = 3$. The corresponding quasar number density is $\bar{n} \approx 5.1 \times 10^{-4} h^3 \text{Mpc}^{-3}$, close to that of the “faint” sample.

Following Fry & Colombi (2013), we compute the void probability P_0 , the mean \bar{N} and the variance in excess of Poisson $\bar{N}^2 \bar{\xi}_2 = \langle N^2 \rangle - \bar{N}^2 - \bar{N}$ from non-overlapping cells with radius in the range $R = 1 - 40 h^{-1} \text{Mpc}$. The uncertainty on χ is calculated following the prescription of Colombi, Bouchet & Schaeffer (1995). While Fig.1 clearly shows that, for the “faint” samples, the data closely follows the NB scaling, there is compelling evidence that the void scaling function of the “bright” sample lies between the NB and GH scalings, despite the lack of data for $\bar{N} \bar{\xi}_2$ much larger than unity. Notwithstanding, our measurements strongly suggest that the void scaling function of quasars also follows the hierarchical pattern, but the scaling may depend on the details of the quasars demographics. We will henceforth assume that it is well represented by the NB model around $z = 3$. We thus expect random dilutions of the quasars population to preserve the NB scaling.

As a consistency check, we have also computed χ for the low redshift haloes that host luminous red galaxies (LRGs), i.e. the $z = 0$ haloes with $M > 5 \times 10^{12} M_{\odot}/h$.

We have found that their void scaling function is better represented by the GH model, in agreement with the findings of Fry & Colombi (2013). In all cases, the various measurements converge towards the Poisson value $\chi \equiv 1$ in the limit $\bar{N}\bar{\xi}_2 \ll 1$ (i.e. infinitesimal cell radius), as expected.

2.4 UVB fluctuations in hierarchical models

The hierarchical ansatz holds regardless the shape of the window function that defines the cell of volume V as long as it decays sufficiently rapidly to zero for large \mathbf{x} . This suggests that we could also assume some sort of hierarchical scaling for the weighted void probability $\mathcal{W}_\omega(V)$ since the window function is effectively

$$\Theta_H(|\mathbf{x}| - R) (1 - \omega(\mathbf{x})) . \quad (22)$$

The term $1 - \omega(\mathbf{x})$ will always suppress the contribution of regions with $|\mathbf{x}| \gg 1$, even when the cell size R is very large. For concreteness, let us have a closer look at the effective volume

$$V_e(s, V) \equiv \int d^3\mathbf{x} (1 - \omega(\mathbf{x})) W_T(\mathbf{x}, V) , \quad (23)$$

which is the relevant quantity in our calculation of UV background fluctuations. Following Meiksin & White (2003), we introduce the normalized specific intensity $j = J/J^*$, with $J^* = L^*/(4\pi r_0)^2$, the optical depth $\tau = r/r_0$ at a distance r from the source and the average number of ionizing sources $\bar{N}_0 = (4\pi/3)r_0^3\bar{n}$ within an attenuation volume. The effective volume becomes

$$\begin{aligned} V_e(s, V) &\equiv \int_0^{R/r_0} d\tau \frac{dV_e}{d\tau}(s, \tau) \\ &= 3 \left(\frac{\bar{N}_0}{\bar{n}} \right) \int_0^{R/r_0} d\tau \tau^2 \\ &\quad \times \int_{\alpha_{\min}}^{\alpha_{\max}} d\alpha \phi(\alpha) \left(1 - e^{-s\alpha\tau^{-2}e^{-\tau}} \right) . \end{aligned} \quad (24)$$

where R is the radius of the tophat filter and the extra factor of J^* as been absorbed into the redefinition $s \rightarrow sJ^*$. The top panel of Fig.2 displays the behaviour of $dV_e/d\tau$ as a function of optical depth for a few choices of s . For illustration purposes, $dV_e/d\tau$ is plotted in unit of $3\bar{N}_0/\bar{n}$ assuming the usual double powerlaw form for the quasar luminosity function (see Eq. 50). $dV_e/d\tau$ reaches a global maximum and decays as $\exp(-\tau)$ in the limit $\tau \gg 1$, suggesting indeed that the hierarchical approximation holds also when the sources are weighted by their contribution to the specific intensity at $\mathbf{x} = 0$.

Therefore, under the assumption that the hierarchical ansatz discussed above also applies for the weighted tophat window $\Theta_H(|\mathbf{x}| - R)(1 - \omega(\mathbf{x}))$, the probability distribution $P(j) = P(J)J^*$ for the normalized specific intensity j is

$$P(j) = \frac{1}{2\pi i} \int_{-i\infty}^{+i\infty} ds e^{sj + \mathcal{W}_\omega(V)} , \quad (25)$$

with a weighted, conditional void probability given by

$$\mathcal{W}_\omega(V) = \sum_{k=1}^{\infty} \frac{(-\bar{N}_e)^k}{k!} \bar{\xi}_k(V_e) \equiv -\bar{N}_e \chi[\bar{N}_e \bar{\xi}_2(V_e)] . \quad (26)$$

$\bar{N}_e = \bar{n}V_e$ is the mean number count in the effective volume

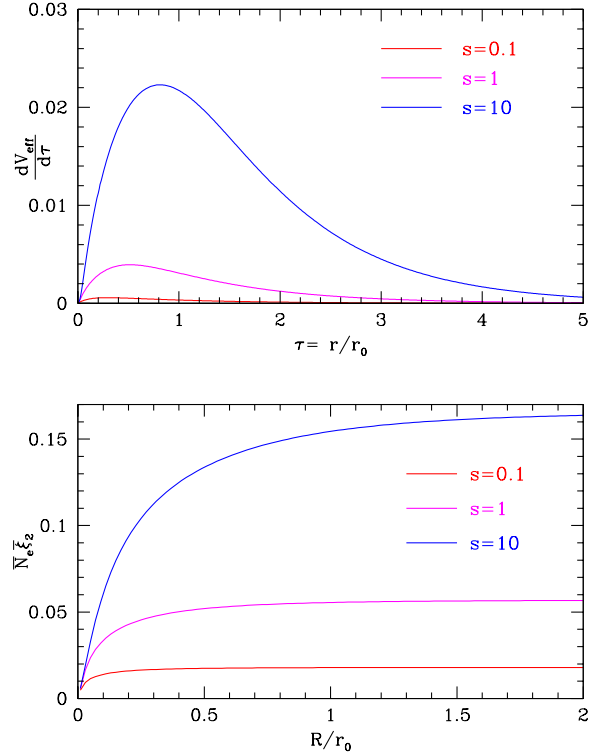


Figure 2. *Top panel* : Differential effective volume $dV_e/d\tau(s, \tau)$ (in unit of $3\bar{N}_0/\bar{n}$) as a function of the optical depth $\tau = r/r_0$. *Bottom panel* : Average clustering strength $\bar{N}_e \bar{\xi}_2$ (in unit of $3\tau_0^\gamma \bar{N}_0$) as a function of the dimensionless cell radius R/r_0 . Results are shown for three different values of s assuming the two-powerlaw form Eq.(50) for the quasar luminosity function, and a powerlaw correlation function with logarithmic slope $\gamma = 1.9$ (color online).

V_e and

$$\begin{aligned} \bar{N}_e \bar{\xi}_2 &\equiv \left(\frac{\bar{n}}{V_e} \right) \int d^3\mathbf{x}_1 \int d^3\mathbf{x}_2 \xi_2(\mathbf{x}_1, \mathbf{x}_2) (1 - \omega(\mathbf{x}_1)) \\ &\quad \times (1 - \omega(\mathbf{x}_2)) \Theta_H(|\mathbf{x}_1| - R) \Theta_H(|\mathbf{x}_2| - R) \end{aligned} \quad (27)$$

is the corresponding integrated clustering strength.

Consider the large bubble limit $R \gg r_\xi$, where r_ξ is the characteristic clustering length of the sources, so that the volume-average 2-point correlation function is approximately $\bar{\xi}_2 \sim V^{-1} \int_V d^3\mathbf{x} \xi_2(r)$. In this regime,

$$\begin{aligned} (\bar{N}_e \bar{\xi}_2)(s) &\approx 3\bar{N}_0 \int_{\alpha_{\min}}^{\alpha_{\max}} d\alpha \phi(\alpha) \\ &\quad \times \int_0^{R/r_0} d\tau \tau^2 \xi(\tau) \left(1 - e^{-s\alpha\tau^{-2}e^{-\tau}} \right) . \end{aligned} \quad (28)$$

For a powerlaw 2-point correlation $\xi_2(r) = (r/r_\xi)^{-\gamma}$, $\bar{N}_e \bar{\xi}_2$ saturates in the limit $R/r_0 \gg 1$ as can be seen in the bottom panel of Fig. 2, where $\bar{N}_e \bar{\xi}_2$ is shown in unit of $3\tau_0^\gamma \bar{N}_0$. Furthermore, $\bar{N}_e \bar{\xi}_2$ increases with s , the variable conjugate to j . We thus naively expect that clustering effects shall be large for $j \ll 1$, but relatively small for $j \gg 1$ since the product $\bar{N}_e \bar{\xi}_2$ saturates rapidly when $s \ll 1$.

Eqs. (25) – (27) are the main result of this Section. We will now explore the behaviour of $P(j)$ in the regime

$j \ll 1$ and $j \gg 1$ before discussing its practical (numerical) implementation.

3 ASYMPTOTICS AND NUMERICS

3.1 Asymptotic expressions

Inverse Laplace transforms are notoriously difficult to perform. Nevertheless, we can use the saddle point approximation to derive closed analytic expressions for the low- and high-intensity tails. Our analysis proceeds along the lines of Bernardeau & Kofman (1995); Colombi et al. (1997); Valageas (2002); Valageas & Munshi (2004); Bernardeau, Pichon & Codis (2013). As will be shown shortly, there is a critical intensity j_c such that, for $j \ll j_c$, the saddle point dominates the contribution to the integral whereas, for $j \gg j_c$, it is the critical point that controls the asymptotic behaviour. For illustration purposes, we will only consider the limit $V \rightarrow \infty$, but the same conclusions hold for finite bubble radii. Details of the calculation can be found in Appendix §B.

3.1.1 Random sources

We begin with the simpler case of randomly-distributed sources. The weighted conditional void probability reduces to $\mathcal{W}_\omega(V) \equiv -\bar{n}V_e(s, V)$. Integrating over the optical depth by parts in Eq.(24) and subsequently taking the limit $V \rightarrow \infty$, we arrive at (Meiksin & White 2003)

$$V_e(s, V \rightarrow \infty) = s \left(\frac{\bar{N}_0}{\bar{n}} \right) \int_{\alpha_{\min}}^{\alpha_{\max}} d\alpha \alpha \phi(\alpha) h(-s\alpha), \quad (29)$$

where the function $h(x)$ is

$$h(x) \equiv \int_0^\infty d\tau \exp(x\tau^{-2}e^{-\tau}) e^{-\tau} (2 + \tau). \quad (30)$$

Performing the inversion $s \rightarrow -s$ through the origin in Eq.(25)¹, the probability distribution for the normalized intensity j takes the form

$$P(j) = \frac{1}{2\pi i} \int_{-i\infty}^{+i\infty} dz e^{-zj+G(z)}, \quad (31)$$

with

$$G(z) = -\bar{N}_e(s = -z) = z\bar{N}_0 \int_{\alpha_{\min}}^{\alpha_{\max}} d\alpha \alpha \phi(\alpha) h(z\alpha). \quad (32)$$

The function $G(z)$, where $z = x + iy$ is the complex variable, is the continuation of $\mathcal{W}_\omega(V)$ over the complex plane. G is analytic everywhere except along the positive real axis $x > 0$ where it is not defined, and it has a branch point at $z = 0$ where $G(0) = 0$. On the negative real axis, $G(x)$ is a convex, monotonically increasing function of x , i.e. $G(x) \leq 0$ for $x \leq 0$.

The argument of the exponential in Eq.(31) admits a saddle point along the negative real axis of the complex

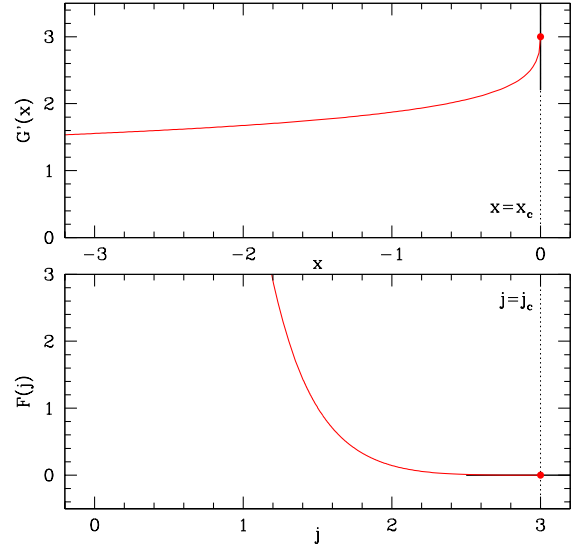


Figure 3. Graph of the first derivative of $G(x)$ (top panel) and its Legendre transform $F(j)$ (bottom panel) near the critical point $(x, j) = (x_c, j_c)$. Both $G(x)$ and $F(j)$ have the same convexity.

plane which is amenable to a stationary phase (or steepest descent) calculation if

$$\frac{\partial}{\partial x}(-xj + G(x)) = 0 \quad (33)$$

$$\frac{\partial^2}{\partial x^2}(-xj + G(x)) > 0 \quad (34)$$

The first condition implies $j = G'(x)$. As shown in the top panel of Fig.3, it can be satisfied for $j \leq j_c$ solely, where the critical intensity $j_c = 3\bar{N}_0\langle\alpha\rangle \equiv \langle j \rangle$ is also the mean specific intensity (Meiksin & White 2003). The second condition guarantees that the real part $G(x)$ goes through a local maximum when z varies perpendicular to the real axis. This must be true since $G(x)$ is convex over the whole negative real axis.

Consider $j < j_c$ and let $(x_s, 0)$ (with $x_s < 0$) be the coordinate of the corresponding saddle point in the complex plane. We can expand $-zj + G(z)$ along the path $z = x_s + iy$ for small $|y| \ll 1$:

$$-jz + G(z) \approx -jx_s + G(x_s) - \frac{1}{2}G''(x_s)y^2 + \dots \quad (35)$$

where a prime denotes a derivative w.r.t. the variable x , and we have used the fact that the real and imaginary part of G are harmonic. At this point, it is convenient to introduce an auxiliary function $F(j)$ defined as the Legendre transform of $G(x_s)$, i.e.

$$F(j) + G(x_s) = jx_s \quad (36)$$

with $j = G'(x_s)$ and $x_s = F'(j)$. Differentiating Eq.(36) w.r.t. to j or x_s , we recover the well-known relation $G''(x_s) = F''(j)^{-1}$. Hence, we can also write $-jz + G(z) \approx -F(j) - y^2/(2F''(j))$. Taking the constant piece out of the inverse Laplace transform and performing the remaining Gaussian integral over y , we obtain the usual formula

$$P(j) \approx \sqrt{\frac{F''(j)}{2\pi}} e^{-F(j)}. \quad (37)$$

¹ The purpose of this inversion is to deal with Legendre transforms of convex rather than concave functions, see below.

Finally, taking the limit $(x, j) \rightarrow (-\infty, 0)$ and using the Legendre transform to solve for $x(j)$, we arrive at (see Appendix §B1)

$$P[\ln(j/j_c)] = -\sqrt{\frac{3\bar{N}_0}{2\pi}} (\ln(j/j_c))^{-1} e^{\bar{N}_0 \ln^3(j/j_c)}, \quad (38)$$

where $P(\ln j) = jP(j)$. Even though this expression is only valid in the limit of small intensities, we shall expect a sharp cutoff when $j \lesssim j_c$. This is clearly seen in Fig. 4.

When $j > j_c$, the contour in the complex plane is pushed along the real positive axis, and wraps around the critical point $z_c = 0$ where the second derivative $G''(x)$ becomes singular. In this case, the trick consists in expanding $F(j)$ around j_c (see the bottom panel of Fig. 3) rather than $G(x)$ around $x_c = 0$, and exploiting the fact that both functions are Legendre transforms of each other to derive an expression for $G(x)$ valid around x_c . We retain only the dominant singular contribution to G to obtain the leading contribution to $P(j)$. The argument of the exponential admits the series expansion (see Appendix §B2)

$$-zj + G(z) = -(j - j_c)z - \frac{2}{3}\sqrt{\frac{2}{f_3}}z^{3/2} + \dots \quad (39)$$

where $f_3 \equiv F^{(3)}(j_c)$ is a negative real number. Subleading contributions scale as z^2 , $z^{5/2}$ etc. On performing the integral in the complex plane, we arrive at

$$P(j) \approx \frac{1}{\sqrt{2\pi}} (j - j_c)^{-5/2} \text{Im}(-f_3^{-1/2}). \quad (40)$$

Lastly, we compute f_3 by taking advantage of relations between the derivatives of the Legendre transforms F and G . We find $f_3 = -(2/9\pi)(\bar{N}_0\langle\alpha^{3/2}\rangle)^{-2}$, so that

$$P(j) \approx \frac{3}{2}\bar{N}_0\langle\alpha^{3/2}\rangle (j - j_c)^{-5/2}. \quad (41)$$

This scaling agrees with that found by Meiksin & White (2003) except for an additional, multiplicative factor of 2.

3.1.2 Clustered sources

As seen in Sec. §2, source clustering can be taken into account upon assuming that the conditional void correlation is of the form Eq.(16). In this case, we can perform an analysis similar to the random case if we define

$$P(j) = \frac{1}{2\pi i} \int_{-i\infty}^{+i\infty} dz e^{-zj + \mathcal{G}(z)} \quad (42)$$

$$\mathcal{G}(z) = G(z)\chi(z), \quad (43)$$

where $G(z)$ is given by Eq.(32) and $\chi(z) = \chi[\bar{N}_e\bar{\xi}_2(s = -z)]$. Hence, it is sufficient to study the behaviour of the void scaling function $\chi(z)$ in order to ascertain the impact of source clustering on the low- and high-intensity tail of the distribution. We clearly have $\chi(z) \rightarrow 1$ when we approach the critical point $z_c = 0$. Furthermore, on the negative real axis, $\chi(x)$ is a monotonically increasing function of x that vanishes in the limit $x \rightarrow -\infty$.

For any choice of $j < j_c$, $\mathcal{G}(x)$ also exhibits a saddle-point on the negative real axis. However, since $0 < \chi(x) < 1$ is monotonically increasing, the saddle-point position $(x_s, 0)$ in the complex plane is closer to the origin than for randomly-distributed sources. As a result, $-F(j) = -x_s j + G(x_s)$ is less negative. Therefore, we also expect a cutoff

at low intensities, but it should occur at relatively smaller values of j . For a powerlaw correlation $\xi_2(r) = (r/r_\xi)^{-2}$, a quick computation yields

$$P(j) \sim \exp\left[-\frac{1}{3\tau_\xi^2} \ln^2\left(\frac{3\tau_\xi^2 j}{2\langle\alpha\rangle}\right)\right], \quad (44)$$

where $\tau_\xi \equiv r_\xi/r_0$ is the source correlation length r_ξ in unit of the attenuation length. Clearly, a slight increase in r_ξ will result in a large amplification of the probability $P(j)$ owing to the exponential factor. Moreover, the dependence on $\ln^2(j)$ rather than $\ln^3(j)$ suggests that the cutoff is not as sharp as in the random case.

Source clustering also affects the amplitude of the distribution in the high-intensity regime. For the powerlaw correlation $\xi_2(r) = (r/r_\xi)^{-2}$, we find

$$P(j) \approx \frac{3}{2} (1 + A\bar{N}_0\tau_\xi^2) \bar{N}_0\langle\alpha^{3/2}\rangle (j - j_c)^{-5/2}, \quad (45)$$

where the coefficient A is proportional to moments of the source luminosity function. A simple approximation to the average clustering strength $(\bar{N}_e\bar{\xi}_2)(s = -z)$ around $z = 0$ leads to $A = (9/4)\langle\sqrt{\alpha}\rangle\langle\alpha\rangle/\langle\alpha^{3/2}\rangle$.

3.2 The mean intensity

The mean specific intensity $\langle j \rangle$ does not change if source clustering is turned on, regardless the value of R . To see this, we write $\langle j \rangle = \int dj jP(j)$, substitute Eq.(42) and integrate je^{-zj} by part. We are thus left with

$$\langle j \rangle = \frac{1}{2\pi i} \int_{\gamma-i\infty}^{\gamma+i\infty} dz \frac{e^{\mathcal{G}(z)}}{z^2} = \text{Res}\left(z^{-2}e^{\mathcal{G}(z)}, z=0\right). \quad (46)$$

Since $\mathcal{G}(z) \approx 3\bar{N}_0\langle\alpha\rangle(1 - e^{-R/r_0})z + \mathcal{O}(z^{3/2})$ in the limit $z \rightarrow 0$, the residue is always $3\bar{N}_0\langle\alpha\rangle(1 - e^{-R/r_0})$, i.e. the mean intensity for a bubble radius R (Meiksin & White 2003). This demonstrates our assertion.

3.3 Numerical implementation

In what follows, we use the Fourier transform to evaluate the probability distribution $P(j)$ numerically. Symmetry considerations show that $P(j)$ is equal to the real part of Eq.(14),

$$P(j) = \frac{1}{\pi} \int_0^\infty ds \cos(-sj + \text{Im } \mathcal{G}(-s)) \times \exp(\text{Re } \mathcal{G}(-s)). \quad (47)$$

Even though the integrand is highly oscillatory at large s , its envelop is damped exponentially in this regime as $\text{Re } \mathcal{G}(-s) \rightarrow -\infty$ in the limit $s \rightarrow \infty$. Therefore, the integral converges very well even when j is significantly larger than j_c . In practice, we sample the real and imaginary part of $\mathcal{W}_\omega(V)$ evenly in $\log(s)$ with $\mathcal{O}(10)$ points per decade from $s = 10^{-5}$ to $s = 10^3$. We use the VEGAS Monte-Carlo algorithm (Lepage 1978) to evaluate the 5-dimensional integrated clustering strength Eq.(27). We subsequently perform the integral over s using a Gauss-Konrod quadrature. Note that

$$\int_{-1}^{+1} d\mu (\tau_1^2 + \tau_2^2 - 2\tau_1\tau_2\mu)^{-\gamma/2} = \frac{(\tau_1 + \tau_2)^{2-\gamma} - |\tau_1 - \tau_2|^{2-\gamma}}{(2-\gamma)\tau_1\tau_2}, \quad (48)$$

which can be used to reduce the dimensionality of the integral Eq.(27) in the case of a powerlaw correlation function $\xi_2(r) = (r/r_\xi)^{-\gamma}$.

To test the accuracy of our numerical results, especially for values of $j \ll j_c$ where the impact of source clustering is expected to be most significant, we also compute $P(j)$ from the inverse Laplace transform Eq.(13). In practice, we begin by inverting the relation $j = \mathcal{G}'(z)$ to locate the saddle point $z = x_s$ on the negative real axis, and then build a path of constant phase in the complex plane upon imposing the condition

$$\delta(-zj + \mathcal{G}(z)) \in \mathbb{R} \quad (49)$$

for each infinitesimal step δz (see e.g. Colombi et al. 1997; Valageas 2002; Bernardreau, Pichon & Codis 2013, for similar constructions). We use the adaptive, multi-dimensional algorithm CUBATURE (Berntsen, Espelid & Genz 1991) to compute $\mathcal{G}(z)$ and its first derivative. The computation of $\mathcal{G}'(z)$ slows down the Laplace transform considerably relative to the Fourier transform.

4 RESULTS

In this Section, we discuss the effect of source clustering on the probability density $P(j)$. For the sake of illustration, we consider the effect of quasar clustering on fluctuations in the HeII-ionizing background at the end of helium reionization ($z \sim 3$). We shall make a few simplifying assumptions here as our goal is not to model the intergalactic medium in detail, but merely obtain a reasonable estimate of the effect. We defer a more detailed study to future work.

4.1 Model inputs: quasars and the IGM

We need to determine three quantities in order to calculate the probability $P(j)$ of the HeII-ionizing radiation: the quasar luminosity function $\Phi(L, z)$, the quasar 2-point correlation function $\xi_2(r)$ and the attenuation length r_0 of the HeII ionizing photons.

A finite cell radius R implies that only a finite number of sources can illuminate a random field point. This happens prior to the completion of helium reionization, when the ionized bubbles around quasars are surrounded by neutral gas which absorbs the radiation emitted by sources outside the local region (see e.g. Furlanetto 2009). Since we consider the end of helium reionization, R is formally infinite. In practice, we shall take $R = 1000$ much larger than the values of r_0 considered.

4.1.1 Quasar luminosity function

We parametrize the bolometric quasar luminosity function (QLF), which we define as the differential comoving number density of quasars with bolometric luminosity L and redshift z , with the standard double powerlaw form (e.g. Boyle, Shanks & Peterson 1988; Boyle et al. 1993; Pei 1995; Croom et al. 2004),

$$\Phi(L, z) = \frac{\Phi_*(z)/L_*(z)}{(L/L_*(z))^{\beta_1(z)} + (L/L_*(z))^{\beta_2(z)}}, \quad (50)$$

where Φ_* is a normalization, $\beta_1(z)$ and $\beta_2(z)$ are the faint- and bright-end slopes of the distribution, respectively, and the characteristic luminosity $L^*(z)$ marks the break from a shallow to a steep slope. Eq.(50) furnishes a good representation of the observations if one allows Φ_* , β_1 , β_2 and L_* to vary with redshift. We use the best-fit values inferred by Hopkins, Richards & Hernquist (2007) for the quasar bolometric QLF at $z = 3$, i.e.

$$\begin{aligned} \Phi_* &= 2.56 \times 10^{-6} \text{ Mpc}^{-3} \\ L_* &= 10^{13.17} L_\odot \\ \beta_1 &= 1.395 \\ \beta_2 &= 3.10 \end{aligned} \quad (51)$$

The normalized, dimensionless quasar number density $\phi(\alpha)$ is constructed from $\Phi(L, z)$ from the relation (Meiksin & White 2003)

$$\phi(\alpha) = \frac{\Phi(\alpha L^*) L^*}{\int_{L_{\min}}^{L_{\max}} dL \Phi(L)}. \quad (52)$$

At the bright end, the number density of quasars diminishes so rapidly that the exact value of L_{\max} has little impact on the results. However, the integral is quite sensitive to L_{\min} owing to the much shallower faint-end slope. In what follows, we will assume $L_{\max} = 5 \times 10^{14} L_\odot$ and $L_{\min} = 10^{10} L_\odot$. This yields a total quasar number density of $\bar{n} \approx 10^{-4} \text{ Mpc}^{-3}$, while the abundance of $L > L_*$ quasars is only $\approx 8 \times 10^{-7} \text{ Mpc}^{-3}$.

At this point, we should in principle convert the bolometric quasar luminosity L into an ionizing intensity at the frequencies of interest (i.e. $h\nu \geq h\nu_{\text{HeII}} = 54.4 \text{ eV}$) assuming, for instance, that the quasar spectral energy distribution follows the broken powerlaw template of Madau, Haardt & Rees (1999). However, since our main objective is to illustrate the applicability of our count-in-cell approach, we will ignore this conversion and only present distributions for the normalized intensity $j = J/J_*$. In doing so, we do not take into account the scatter in the far-UV spectral index (Telfer et al. 2002; Desjacques, Nusser & Sheth 2007). Nevertheless, this should have a negligible impact on the intensity distribution $P(j)$ (see Fig.1 of Furlanetto 2009).

4.1.2 Quasar clustering

The real-space 2-point correlation function of quasars is often fitted to a powerlaw of the form $\xi_2(r) = (r/r_\xi)^{-\gamma}$. A number of studies have explored the clustering of high-redshift quasars, but their clustering amplitude is still a matter of debate. Early estimates based on the incidence of close quasar pairs set lower limits to the correlation length of $r_\xi \gtrsim 15 - 20 \text{ Mpc}$ (Stephens et al. 1997; Kundić 1997; Schneider et al. 2000; Djorgovski et al. 2003). In a more recent analysis based on a sample of 4462 quasars in the redshift range $2.9 \leq z \leq 5.4$, Shen et al. (2007) obtained $r_\xi \sim 21 \text{ Mpc}$ assuming a powerlaw slope $\gamma \sim 2$, with a strong indication that the high-redshift quasars with $z \geq 3.5$ are substantially more clustered ($r_\xi \sim 35 \text{ Mpc}$). Francke et al. (2008) found a similar, albeit smaller value of $r_\xi \sim 14 \text{ Mpc}$ from a measurement of the cross-correlation between Lyman Break Galaxies (LBGs) and quasars in the redshift range

$2.7 < z < 3.8$. In what follows, we will fix the powerlaw slope to $\gamma = 2.1$, but let the correlation length vary generously around the fiducial value of $r_\xi = 15$ Mpc. Furthermore, we shall assume that the quasar void scaling function follows hierarchical clustering, i.e. $\chi = \chi(\bar{N}\xi_2)$, and is well represented by the Negative Binomial model discussed above. Note that χ needs not be universal. Our approximation would indeed work even if χ depends on redshift because the attenuation length r_0 is considerably smaller than the Hubble time t_H . However, it is crucial that χ be a function of the integrated clustering strength $\bar{N}\xi_2$ only.

These analyzes also suggest that quasar clustering strongly depends on luminosity at high redshift, in agreement with various theoretical predictions (Porciani, Magliocchetti & Norberg 2004; Hopkins, Richards & Hernquist 2007; Croton 2009). Even though our procedure ignores this possibility, we stress that the model of Croton (2009) predicts a linear bias $b_1 \sim 6 - 9$ (assuming $\sigma_8 = 0.9$) for the $z = 3$ quasars shining at the characteristic luminosity L_* , consistent with our choice of $r_\xi = 15$ Mpc for the fiducial quasar correlation length.

4.1.3 Attenuation length and cell size

The (comoving) attenuation length of HeII-ionizing photons is a crucial ingredient of our model. Following Furlanetto (2009); Dixon & Furlanetto (2009), we shall ignore variations in the sight line opacity and any frequency-dependence in order to characterize this attenuation through a single number r_0 . Estimations based on the incidence of Lyman-limit systems (Bolton et al. 2006) or the propagation of ionizing photons around individual quasars (Furlanetto & Oh 2008) indicate that the average attenuation length at $z = 3$ is $r_0 \sim 30 - 40$ Mpc, while the more sophisticated treatment of Davies & Furlanetto (2014) yields a somewhat larger value, $r_0 \sim 60$ Mpc. To be conservative, we will consider a couple of attenuation lengths in addition to the fiducial value of 35 Mpc so as to brackets the aforementioned estimates.

4.2 Intensity distribution in a fully ionized IGM

Fig.4 illustrates the effect of quasar clustering on the distribution of HeII-ionizing intensity for an attenuation length $r_0 = 35$ Mpc. All the distributions have been computed using the Fourier transform Eq.(14). For comparison, the data point have been obtained from the Laplace transform Eq.(13) using the saddle point approximation described in §3.1. The good agreement between the two methods demonstrates that our numerical evaluation of $P(j)$ is robust. The dashed line is for randomly distributed quasars, whereas the solid curves show $P(j)$ for a quasar correlation length in the range $5 < r_\xi < 30$ Mpc (increasing from the narrowest to the widest distribution). Clustering widens the distribution at small j essentially because source correlations substantially increases the probability of findings regions devoid of quasars. The effect becomes significant when $r_\xi \gtrsim 15$ Mpc for the attenuation length adopted here. At high intensity, the various distribution converge towards the scaling $P(j) \sim j^{-5/2}$. The amplitude increases with clustering strength, in agreement with our asymptotic expectation

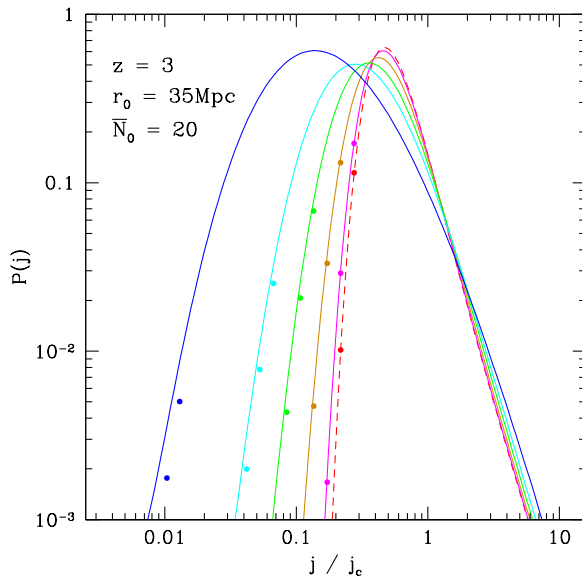


Figure 4. The probability distribution $P(j)$ of the HeII-ionizing intensity (in unit of j_c) in the reionized IGM. The attenuation length is $r_0 = 35$ Mpc and the QLF is the standard double powerlaw Eq.(50). The dashed curve is for randomly distributed quasars, whereas the solid curves assume a powerlaw correlation with correlation length $r_\xi = 5, 10, 15, 20$ et 30 Mpc from narrowest to widest, respectively. The data points have been obtained upon applying the saddle point approximation to the Laplace transform Eq.(13), and are in good agreement with the various curves, which have all been computed using the Fourier transform Eq.(14) (color online).

Eq.(45). The probability to have an intensity $j \gtrsim 3j_c$ is $\sim 17\%$ (resp. 80%) larger for $r_\xi = 15$ Mpc (resp. $r_\xi = 30$ Mpc) relative to randomly distributed quasars. This fairly weak enhancement is consistent with a value of $A \approx 0.05$ in Eq.(45) much smaller than $A = (9/4)\langle\sqrt{\alpha}\rangle\langle\alpha\rangle/\langle\alpha^{3/2}\rangle \approx 0.3$ expected for the QLF adopted here.

The high-intensity scaling $P(j) \sim j^{-5/2}$ reflects the behaviour of the nearest neighbour probability density,

$$H_1(r)dr = -\frac{\partial P_0}{\partial r}dr = \frac{\partial(\bar{N}\chi)}{\partial r}e^{-\bar{N}\chi}dr. \quad (53)$$

Consider indeed that all the quasars shine with a luminosity $L = L_*$. Ignoring the attenuation of ionizing photons, the optical depth scales as $\tau = (J_*/J)^{1/2} = j^{-1/2}$. For a random distribution,

$$H_1(\tau)d\tau = 3\bar{N}_0\tau^2e^{-\bar{N}_0\tau^3}d\tau \quad (54)$$

and is, of course, normalized to unity: $\int d\tau H_1(\tau) = 1$. On inserting $\tau = j^{-1/2}$ into this expression, we derive a probability density

$$P(j)dj = \frac{3}{2}\left(\frac{\bar{N}_0}{j^{5/2}}\right)e^{-\bar{N}_0/j^{3/2}}dj \quad (55)$$

for the ionizing intensity. Finally, replacing \bar{N}_0 by $\bar{N}_0\langle\alpha^{3/2}\rangle$ yields the scaling Eq.(41). This scaling persists in the clustered case since, in the limit $\tau \ll 1$, the nearest neighbour distribution is insensitive to the amplitude of clustering. Most importantly however, the amplitude increases with the clustering strength as discussed above, presumably because

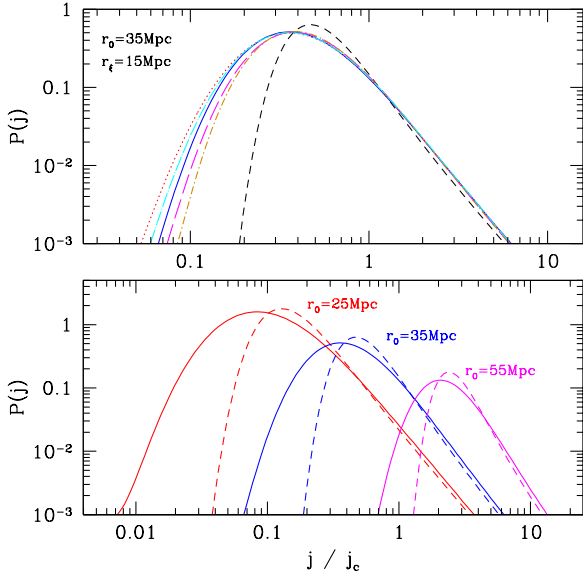


Figure 5. *Top panel* : Effect of changing the behaviour of the quasar correlation function on the distribution $P(j)$. The solid (blue) curve is our fiducial model, the dotted (red) curve was obtained using the GH rather than the NB void scaling function, the long-dashed (magenta) curve has $\xi_2 = 0$ for $r < 1$ Mpc while the dotted-short dashed (orange) assumes $\xi_2 = 0$ outside the range $1 < r < 150$ Mpc. Finally, the dotted-long dashed (cyan) curve assumes a powerlaw slope $\gamma = 1.9$ rather than 2.1. The correlation and attenuation lengths are $r_\xi = 15$ Mpc and $r_0 = 35$ Mpc, respectively. *Bottom panel* : $P(j)$ for 3 different attenuation lengths. Results are shown for randomly distributed (dashed curves) and clustered sources with $r_\xi = 15$ Mpc (solid curves).

finding the second-nearest neighbour close to the first one is more likely.

We have thus far assumed that the quasar 2-point correlation follows a powerlaw at all separations, even though we expect quasars to be anti-correlated at very large scales. Furthermore, if quasars populate distinct haloes, then we should also expect anti-correlation at separations $r \lesssim 1$ Mpc smaller than the typical halo size. In order to gauge the importance of these effects, the top panel of Fig.5 displays the distribution $P(j)$ for the fiducial powerlaw scaling, yet assuming $\xi_2(r) = 0$ at short separations $r < 1$ Mpc (long-dashed curve), as well as outside the range $1 < r < 150$ Mpc (dotted-dashed curve). In this case, we have checked that setting $\xi_2 = -0.001$ or -0.01 for $r > 150$ Mpc does not change $P(j)$ appreciably. We also show the impact of changing the void scaling function from the fiducial NB scaling to the GH model (dotted curve), and raising the powerlaw slope from $\gamma = 1.9$ to 2.1 (dotted-long dashed curve). Overall, the low-intensity tail is quite sensitive to variations in the default assumptions, with up to an order of magnitude difference in the probability already at $j = 0.1j_c$. By contrast, the high-intensity tail is barely affected as it is dominated by the nearest neighbour.

The impact of clustering relative to Poisson fluctuations should diminish as the number density \bar{N}_0 of sources in an attenuation volume decreases. This is indeed the case, as we will see shortly. At low intensities however, the opposite happens. To understand this, consider the GH scaling

Table 1. Variance $\langle \Delta j^2 \rangle$ of intensity fluctuations relative to the Poisson result. Both the quasar clustering length r_ξ and the attenuation length r_0 are in units of (comoving) Mpc.

	$r_\xi = 5$	$r_\xi = 10$	$r_\xi = 15$	$r_\xi = 20$	$r_\xi = 30$
$r_0 = 25$	1.02	1.08	1.19	1.35	1.56
$r_0 = 35$	1.03	1.10	1.23	1.41	1.95
$r_0 = 55$	1.05	1.15	1.32	1.56	2.25

for simplicity. For $j \ll 1$ (i.e. $s \gg 1$), the weighted, conditional void probability \mathcal{W}_ω given by Eq.(26) scales like $-\bar{N}_e \chi(\bar{N}_e \bar{\xi}_2) \sim -\bar{\xi}_2^{-1} \sim -\tau_\xi^{-\gamma}$ when $\bar{N}_e \bar{\xi}_2 \rightarrow \infty$. In other words, \mathcal{W}_ω increasingly deviates from the Poisson results $\sim -r_0^3$, and a larger clustering length further enhances the suppression, in agreement with our asymptotic expression Eq.(44). This is clearly seen in Fig.5, where the intensity distributions for randomly-distributed and clustered sources are compared for three different values of the attenuation length $r_0 = 25, 35$ and 55 Mpc. The number of quasars in an attenuation volume is $\bar{N}_0 \sim 7, 20$ and 76 , respectively. A constant clustering length $r_\xi = 15$ Mpc is assumed for all the solid curves. Note again the enhancement of $P(j)$ at large intensities, which is consistent with Eq.(45) (i.e. the effect increases with $\bar{N}_0 \tau_\xi^2 \sim r_0 r_\xi^2$) provided that $A \approx 0.05$.

To quantify the impact of source clustering on $P(j)$, we have measured the variance of intensity fluctuations, $\langle \Delta j^2 \rangle = \langle j^2 \rangle - \langle j \rangle^2$, relative to the Poisson case for a range of values of r_0 and r_ξ . Results are summarized in Table 1. All the models assume a powerlaw slope $\gamma = 2.1$. As expected, the deviation increases with r_0 or, equivalently, with decreasing Poisson noise. At fixed r_0 , it echoes the rise in the amplitude of the $j^{-5/2}$ tail with increasing correlation length r_ξ .

4.3 Environmental dependence of $P(j)$

We have thus far focused on the distribution $P(j)$ for random field points. Source clustering increases the probability for intensities $j \ll j_c$ because regions devoid of quasars are significantly more abundant. Therefore, we may expect that $P(j)$ depends on whether we sit in a high or low density region.

4.3.1 Spherical collapse considerations

To ascertain the magnitude of this environmental dependence, we restrict the set of field points to those located at the center of spheres of volume $V \propto R^3$ with fractional density δ . The conditional void probability function acquires a dependence on δ ,

$$\begin{aligned} \mathcal{W}_0(V|\delta) &= \sum_{k=0}^{\infty} \frac{(-\bar{n})^k}{k!} \int_V d^3 \mathbf{x}_1 \dots \int_V d^3 \mathbf{x}_k \xi_k(\mathbf{x}_1, \dots, \mathbf{x}_k|\delta) \\ &\equiv \sum_{k=1}^{\infty} \frac{(-\bar{N})^k}{k!} \bar{\xi}_k(V|\delta). \end{aligned} \quad (56)$$

As before, $\mathcal{W}_0(V|\delta)$ generates all the count probabilities subject to the condition that the cell fractional density is δ . In

particular, since $\xi_1(\mathbf{x}|\delta)$ is now different from unity, the average number density of sources in those cells,

$$\langle N|\delta \rangle V^{-1} = \bar{n} V^{-1} \int_V d^3\mathbf{x} \xi_1(\mathbf{x}|\delta), \quad (57)$$

is an decreasing (increasing) function of V if $\delta > 0$ ($\delta < 0$) such that $\langle N|\delta \rangle \rightarrow \bar{n}V$ in the limit of large cell volume. In other words, $\xi_1(\mathbf{x}|\delta) \equiv \xi_1(r|\delta)$ is the average source density profile around a given overdensity δ .

To estimate $\xi_1(r|\delta)$, we use the spherical collapse model, which establishes a connection between the evolved region and the initial seed perturbation (Gunn & Gott 1972; Peebles 1980). Namely, the initial size R_0 and overdensity δ_0 are related to R and δ through (Bernardeau 1994; Mo & White 1996; Sheth 1998)

$$\delta_0 = \delta_c \left[1 - (1 + \delta)^{-1/\delta_c} \right], \quad 1 + \delta = \left(\frac{R_0}{R} \right)^3. \quad (58)$$

Here, δ_0 is the initial density linearly extrapolated to the redshift under consideration, so it can take values less than -1 . These relations can be used to estimate the initial profile $\xi_1(s|\delta_0) = \bar{n}(s|\delta_0)/\bar{n}$ as a function of Lagrangian separation s . Let R_1 be the characteristic Lagrangian radius of the peaks that collapse into the haloes hosting quasars. In the peak-background split approach (Kaiser 1984), density fluctuations in the environment locally modulate the peak number density. Taking into account the non-zero correlation between R_1 and R_0 , the initial profile is

$$\begin{aligned} \xi_1(s|\delta_0) &= \frac{\mathcal{N}(\nu_c|\nu_0, s)}{\mathcal{N}(\nu_c)} \\ &= \exp \left[-\frac{\epsilon^2(s)(\nu_c^2 + \nu_0^2) - 2\epsilon(s)\nu_c\nu_0}{2(1 - \epsilon^2(s))} \right], \end{aligned} \quad (59)$$

where \mathcal{N} is a Normal distribution, $\nu_c = \delta_c/\sigma_1$ is the peak height, $\nu_0 = \delta_0/\sigma_0$ is the significance of the initial large-scale perturbation, and $\epsilon(s) = \sigma_{\times}^2(s)/(\sigma_0\sigma_1)$ is the cross-correlation between the short- and long-wavelength modes. Here, σ_0 and σ_1 are the rms variance of density fluctuations smoothed on scale R_0 and R_1 , respectively, and

$$\sigma_{\times}^2(s) = \frac{1}{2\pi^2} \int_0^\infty dk k^2 P(k) W_T(kR_0) W_T(kR_1) j_0(ks) \quad (60)$$

is a cross-correlation involving one filter of size R_0 and the other of size R_1 . Evolving $\bar{n}(s|\delta_0)$ requires in principle knowledge of the average, initial density profile as a function of s . For simplicity however, we assume that $\xi_1(s|\delta_0)$ evolves in a self-similar way, and convert Lagrangian to Eulerian scales according to $r = (1 + \delta)^{-1/3}s$. Therefore, we compute $\xi_1(r|\delta)$ as

$$\xi_1(r|\delta) = \xi_1(s(r)|\delta_0). \quad (61)$$

Fig.6 displays several profiles obtained for a large-scale environment density $\delta = -2\sigma, -1\sigma, +1\sigma$ and $+2\sigma$ (curves from bottom to top), where σ is the rms variance of the $z = 3$ density field smoothed on comoving scale $R = 28.5$ Mpc. The effect sensitively depends on the choice of ν_c . Dashed and solid curves assume a peak height $\nu_c = 2$ and 3 (obtained upon setting $R_1 = 1.1$ and 3 Mpc), which corresponds to a linear halo bias $b_1 \sim 1 + (\nu_c/\sigma_1) \approx 3.4$ and 6.4, respectively. Low density regions with $\delta = -2\sigma$ hardly contain virialized, $\nu_c = 3$ haloes.

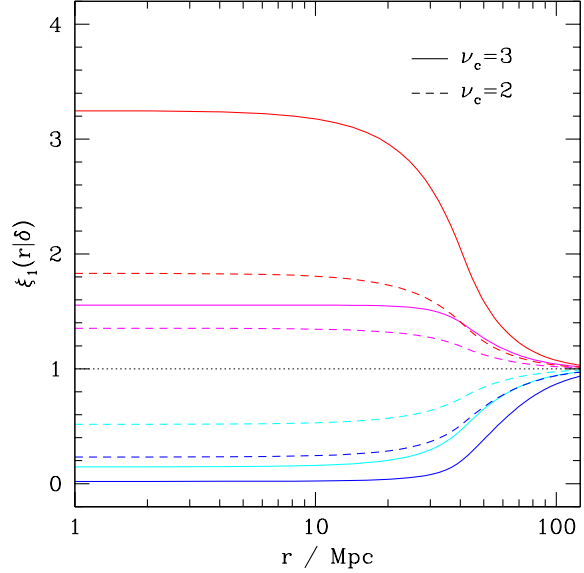


Figure 6. Relative abundance of sources $\xi_1(r|\delta) = \bar{n}(r|\delta)/\bar{n}$ around overdense and underdense regions as a function of comoving distance r . Results are shown for a large-scale environment density $\delta = -2\sigma, -1\sigma, +1\sigma$ and $+2\sigma$ at $z = 3$ (curves from bottom to top), where σ is the rms variance of the evolved density field on comoving scale $R = 28.5$ Mpc. Solid and dashed lines were obtained assuming $\nu_c = 3$ and 2, respectively.

Furthermore, all the higher-order correlations $\bar{\xi}_k(V|\delta)$ are also affected by the environmental constraint. Their δ -dependence could also be worked out using the spherical collapse model. However, since we can only speculate about whether the void scaling function $\chi(r|\delta)$ still satisfies the hierarchical scaling, we will present results assuming $\bar{\xi}_k(V|\delta) = 0$ for $k \geq 3$. Note that the sources are nonetheless clustered to some extent since their number density increases (decreases) in overdense (underdense) regions as exemplified in Fig.6

The top panel of Fig.7 displays the resulting conditional distribution $P(J|\delta)$ given a large-scale environment density $\delta = -2\sigma, 0$ and $+2\sigma$ (dashed, dotted and solid curves, respectively). The corresponding average intensity is $\langle J \rangle \approx 0.96, 2.70$ and 5.84 in unit of $J_{35}^* \equiv J^*(r_0 = 35 \text{ Mpc})$, as is the abscissa of Fig.7. We have assumed $\nu_c = 3$ as above to compute $\xi_1(r|\delta)$, and a fixed attenuation length $r_0 = 35$ Mpc regardless the value of δ . Even though the differences in $P(j)$ are quite significant, they should be regarded as an upper bound since we have considered relatively rare, 2σ fluctuations traced by highly biased sources.

4.3.2 Sensitivity to the clustering of absorption systems

Clearly, the attenuation length must vary spatially since it is mainly determined by the number density of absorption systems. While the absorption systems with low HI column densities (i.e. $\log(N_{\text{HI}}) < 17.2 \text{ cm}^{-2}$) are distributed relatively uniformly, both the Lyman Limit Systems (LLS; $17.2 < \log(N_{\text{HI}}) < 20.3 \text{ cm}^{-2}$) – which correspond to metal line (Mg II, C IV) systems – and Damped Ly α Absorbers (DLA; $\log(N_{\text{HI}}) > 20.3 \text{ cm}^{-2}$) – which trace gas-rich galax-

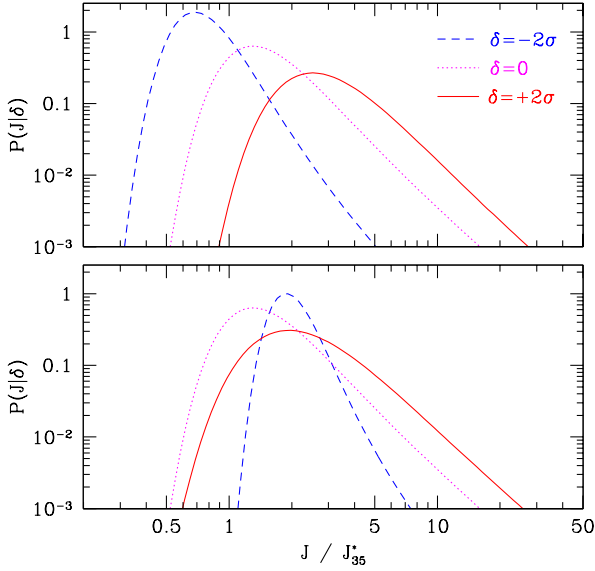


Figure 7. Distribution $P(j)$ as a function of the large-scale environment, characterized by the fractional density δ on comoving scale $R = 20 \ h^{-1}\text{Mpc}$. In the top panel, a constant attenuation length $r_0 = 35 \text{ Mpc}$ is assumed regardless of the large-scale density whereas, in the bottom panel, r_0 is allowed to vary with the local environment density (see text). Note that the specific intensity J is in unit of $J_{35}^* \equiv J^*(r_0 = 35 \text{ Mpc})$.

ies at high redshift – are expected to be noticeably clustered, though likely not as much as quasars. For instance, the recent analysis of Font-Ribera et al. (2012) finds $b_1 \sim 2.2$ for DLAs in the redshift range $2 < z < 3.5$. Clearly, strong absorption systems will be overabundant (underabundant) in regions with $\delta > 0$ ($\delta < 0$). Hence, we might expect a relatively shorter (longer) attenuation length when the ionizing radiation field is seen from the center of an overdense (underdense) region.

The clustering length of absorption systems generally depends on their column density. However, owing to the scarcity of observational constraints, we simply assume that the absorption systems trace the $\nu_c = 2$ peaks discussed above and set the local attenuation length to $r_0(\delta) = r_0 \xi_1(0|\delta)^{-1/3}$ in the computation of $P(j)$. This scaling reflects the fact that $r_0 \propto \bar{n}_{\text{abs}}^{-1/3}$, where \bar{n}_{abs} is the number density of LLS and DLAs. The resulting attenuation length is $\sim 57 \text{ Mpc}$ and $\sim 29 \text{ Mpc}$ for the regions with large-scale density $\delta = -2\sigma$ and $+2\sigma$, respectively. The corresponding intensity distributions are shown in the bottom panel of Fig.7. Unsurprisingly, our spatially-varying prescription for $r_0(\delta)$ reduces differences between the distributions obtained for low and high density regions. Still, the average intensity in $\delta = +2\sigma$ regions remains about twice as large (5.06) as that of random field points. Although a detailed account of the clustering of absorption systems around the sources will be essential to quantify this effect precisely, it is clear that variations in the mean intensity should not exceed a few, even for relatively pronounced overdense or underdense regions.

5 DISCUSSION

To our knowledge, the only study which has thus far addressed the impact of quasar clustering on the post-reionization distribution $P(j)$ is the semi-numerical treatment of Dixon, Furlanetto & Mesinger (2014), in which dark matter haloes are generated upon applying the excursion set approach to realizations of the linear density field in periodic boxes of size $L = 250 \ h^{-1}\text{Mpc}$. Overall, our results are consistent with theirs: clustering widens the intensity distribution and, thus, enhances the probability for $j \ll \langle j \rangle$ and $j \gg \langle j \rangle$. Regarding the magnitude of the effect, the fact that their distributions are nearly identical regardless of whether the sources randomly sample haloes or are randomly distributed suggests that the correlation length r_ξ of their synthetic quasars is fairly small. Furthermore, their fiducial attenuation length is $r_0 = 60 \text{ Mpc}$, about twice as large as ours. The effects shown in Fig.4 would appear smaller, had we adopted the same value of r_0 . Finally, their simulated distributions exhibit a very sharp cutoff at low intensities, presumably because their simulation box is too small to contain a representative sample of those underdense regions responsible for the low-intensity tail.

We have derived asymptotic expressions to further check the validity of our numerical implementation. While our asymptotic scaling are consistent with the impact of source clustering as inferred from the numerical evaluation of $P(j)$, there is a mismatch at high intensities between the predicted and simulated amplitude of the powerlaw tail. Namely, the impact of source clustering is ~ 6 times smaller than the theoretical expectation. We have not been able to understand the origin of this discrepancy, and a more rigorous analysis is beyond the scope of this paper. However, we have numerically checked that, for a fixed r_0 , the mean intensities of the distributions with $0 \leq r_\xi \leq 30 \text{ Mpc}$ agree with each at the 1.5 percent level (large differences would offset the distribution). Therefore, there is no systematic offset along the abscissa. We thus believe that the rise of the high- j amplitude with r_ξ is real, rather than the manifestation of a numerical error.

The main drawback of our method is the absence of a treatment for the small-scale structure of the IGM, radiative transfer effects etc. (see e.g. Maselli & Ferrara 2005; Tittley & Meiksin 2007). Notwithstanding, it has the advantage to be very fast – generate a distribution $P(j)$ takes $\mathcal{O}(20)$ minutes on a standard workstation – and, thus, allows us to explore a wide range of quasar properties and demographics. In the present study, the model inputs are the observed quasar luminosity function and 2-point correlation, but one could instead use predictions based on a halo occupation distribution (HOD). The large scatter in the observed correlation length of high redshift quasars may reflect, at least partly, a luminosity-dependence of quasar clustering. Our approach can be extended to account for this dependence: the source correlations functions could in principle depend on both r and α , and the behaviour of void scaling function could generally be a function of α . Further improvements include a frequency-dependent attenuation length (to account for the longer mean free path of hard photons) and a better modelling of the clustering of absorption systems. Clearly, such analytic approaches will never surpass detailed (and computationally expensive) cosmological hydrodynam-

ical simulations with radiative transfer, but they can furnish useful insights into the effect of discrete, clustered sources and absorbers on the physical state of the high-redshift IGM.

Finally, one should bear in mind the caveat that the weighted void probability follows the hierarchical ansatz (see Sec. §2.4). We have shown that the conditional void correlation of high-redshift mock quasars follows the hierarchical scaling but, in order to fully demonstrate the consistency of our model, we should explicitly check that this remains the case when we weight the sources according to Eq.(12). We intend to test this assumption in a future work.

6 CONCLUSION

We have developed a count-in-cell approach to the distribution of ionizing intensity which includes source clustering. We have applied our method to quantify the impact of quasar clustering on the distribution of HeII ionizing radiation at the end of helium reionization ($z \sim 3$). Our results can be summarized as follows:

- Our approach crucially relies on the assumption that the distribution of ionizing sources follows the hierarchical ansatz. We have tested this hypothesis using catalogues of synthetic quasars at $z \sim 3$. We have found that the void scaling function of these mocks closely tracks the Negative Binomial scaling. Therefore, we have assumed that the real quasars follow the same pattern in all our predictions.

- We have derived asymptotic expectations in the low- and high-intensity regime. We have shown that source clustering can noticeably increase the probability of finding ionizing intensities $j \ll \langle j \rangle$, while it enhances the amplitude of the powerlaw tail $\propto j^{-5/2}$ for $j \gtrsim \langle j \rangle$. We have implemented the numerical computation of the intensity distribution in two different ways to check the robustness of our numerical results.

- Using the observationally determined quasar luminosity function and 2-point correlation, and ignoring any possible luminosity-dependence of quasar clustering, we have found that, for a (comoving) attenuation length in the range $25 < r_0 < 55$ Mpc, quasar clustering becomes significant when the correlation length exceeds $\sim 15 - 20$ Mpc. Overall, the importance of source clustering increases with $\bar{N}_0 \sim (r_0/l)^3$ (smaller Poisson fluctuations) and with r_ξ/r_0 (larger clustering strength).

- We have shown that the distribution of ionizing intensity depends on the surrounding environment. Variations of a few in the mean specific intensity $\langle j \rangle$ are expected for large-scale ($R \sim 30$ Mpc), $\pm 2\sigma$ density fluctuations. However, a better characterization of the connection between quasars and strong absorption systems is in order to make more accurate predictions.

To conclude, quasar clustering is certainly not the dominant source of fluctuations in the distribution of HeII-ionizing intensity at $z \sim 3$. However, owing to the large uncertainties in the attenuation length r_0 and the clustering length r_ξ , it is difficult to draw any firm conclusion about the magnitude of this effect. If $r_\xi \lesssim 15$ Mpc and $r_0 \lesssim 55$ Mpc, then quasar clustering is definitely a secondary source of variance (with a contribution less than $\sim 30\%$), in agreement with the findings of Dixon, Furlanetto & Mesinger (2014). By contrast,

if the attenuation length is on the high side of the allowed range, $r_0 \gtrsim 55$ Mpc, and/or if the clustering of high-redshift quasars has a strong luminosity-dependence, with the rare bright quasars being highly clustered, then the variance of intensity fluctuations may be enhanced quite significantly.

ACKNOWLEDGMENTS

We are grateful to Darren Croton for making his mock quasar catalogues available to us. VD would like to thank the organisers of the Gravasco trimester at the Institut Henri Poincaré for hospitality when parts of this work were being completed; as well as Stéphane Colombi, Ravi Sheth and Patrick Valageas for interesting discussions; and Sandrine Codis for correspondence. MB would like to thank Alba Grassi for useful discussions. VD and MB acknowledge support by Swiss National Science Foundation.

APPENDIX A: GENERATING FUNCTIONAL FOR WEIGHTED PROBABILITIES

We begin with the probability to have a cell of volume V empty of particles except at $N \geq 0$ distinct locations $\mathbf{x}_1, \dots, \mathbf{x}_N$,

$$P\{\Phi_0(V)\} = \exp[W_0(V)] \quad (A1)$$

$$P\{X_1\Phi_0(V)\} = \bar{n}W_1(\mathbf{x}_1; V)d^3\mathbf{x}_1 P\{\Phi_0(V)\}$$

$$P\{X_1X_2\Phi_0(V)\} = \bar{n}^2 \left[W_1(\mathbf{x}_1; V)W_1(\mathbf{x}_2; V) + W_2(\mathbf{x}_1, \mathbf{x}_2; V) \right] d^3\mathbf{x}_1 d^3\mathbf{x}_2 P\{\Phi_0(V)\} \\ \dots$$

Here, W_N is the N -point conditional correlation function (see Eq.(7) of White 1979). Substituting these relations into the series expansion Eq.(6), we obtain

$$P_\omega(V) = \left\{ \bar{n}(\xi_{k+1} \star \omega) + \frac{\bar{n}^2}{2!} \left[(\xi_{k+1} \star \omega)^2 + (\xi_{k+2} \star \omega^2) \right] + \frac{\bar{n}^3}{3!} \left[(\xi_{k+1} \star \omega)^3 + 3(\xi_{k+1} \star \omega)(\xi_{k+2} \star \omega^2) + (\xi_{k+3} \star \omega^3) \right] + \dots \right\} e^{W_0(V)}, \quad (A2)$$

where $(\xi_{k+i} \star \omega^i)$ is a shorthand notation for the infinite sum

$$\sum_{k=0}^{\infty} \frac{(-\bar{n})^k}{k!} \int_V d^3\mathbf{x}_1 \dots \int_V d^3\mathbf{x}_{k+i} \\ \times \xi_{k+i}(\mathbf{x}_1, \dots, \mathbf{x}_{k+i}) \omega(\mathbf{x}_1) \dots \omega(\mathbf{x}_i) \quad (A3)$$

Note that this series involves irreducible correlation functions ξ_N with $N \geq i$ solely. Let us first consider a random distribution, for which $\xi_1(\mathbf{x}) \equiv 1$ only is non-zero. Since $\xi_1(\mathbf{x})$ appears exclusively in $(\xi_{k+1} \star \omega)$, $P_\omega(V)$ simplifies to

$$P_\omega(V) = \left\{ \bar{n} \int_V d^3\mathbf{x} \omega(\mathbf{x}) + \frac{\bar{n}^2}{2!} \left(\int_V d^3\mathbf{x} \omega(\mathbf{x}) \right)^2 + \dots \right\} e^{W_0(V)} \\ = e^{-\bar{n}} \int_V d^3\mathbf{x} (1 - \omega(\mathbf{x})) - e^{-\bar{n}V}. \quad (A4)$$

When the distribution is not Poisson, the first non-trivial correlation is $\xi_2(\mathbf{x}_1, \mathbf{x}_2)$, which contributes two terms at leading (linear) order,

$$-\bar{n}^2 \int_V d^3\mathbf{x}_1 \int_V d^3\mathbf{x}_2 \xi_2(\mathbf{x}_1, \mathbf{x}_2) \omega(\mathbf{x}_1) + \frac{\bar{n}^2}{2!} \int_V d^3\mathbf{x}_1 \int_V d^3\mathbf{x}_2 \xi_2(\mathbf{x}_1, \mathbf{x}_2) \omega(\mathbf{x}_1) \omega(\mathbf{x}_2). \quad (\text{A5})$$

The first arises from $\bar{n}(\xi_{k+1} \star \omega)$ whereas the second appears in $(\bar{n}^2/2)(\xi_{k+2} \star \omega^2)$. This can also be written as

$$\frac{\bar{n}^2}{2!} \int_V d^3\mathbf{x}_1 \int_V d^3\mathbf{x}_2 \xi_2(\mathbf{x}_1, \mathbf{x}_2) \times [\omega(\mathbf{x}_1)\omega(\mathbf{x}_2) - \omega(\mathbf{x}_1) - \omega(\mathbf{x}_2)]. \quad (\text{A6})$$

Furthermore, Taylor expanding the void probability $P_0 = \exp[\mathcal{W}_0(V)]$ brings down an additional factor of

$$\frac{\bar{n}^2}{2!} \int_V d^3\mathbf{x}_1 \int_V d^3\mathbf{x}_2 \xi_2(\mathbf{x}_1, \mathbf{x}_2), \quad (\text{A7})$$

Hence, the terms linear in $\xi_2(\mathbf{x}_1, \mathbf{x}_2)$ are all quadratic in \bar{n} and sum up to

$$\frac{\bar{n}^2}{2!} \int_V d^3\mathbf{x}_1 \int_V d^3\mathbf{x}_2 \xi_2(\mathbf{x}_1, \mathbf{x}_2) (1 - \omega(\mathbf{x}_1)) (1 - \omega(\mathbf{x}_2)). \quad (\text{A8})$$

This suggests replacing Eq.(A4) by Eq.(7), where $\mathcal{W}_\omega(V)$ is given by Eq.(8). Subsequent checks at third order show that this must be the exact result.

APPENDIX B: ASYMPTOTICS

B1 Low-intensity tail

To estimate how $P(j)$ scales in the low-intensity limit, Eq.(37), we need to evaluate $F(j)$ and $F''(j)$. To this purpose, we follow Meiksin & White (2003) and write the function $h(z)$ as

$$h(z) = \int_0^\infty du e^{zu} \tau^3(u), \quad (\text{B1})$$

where $\tau(u)$ is solution of $u = \tau^{-2}e^{-\tau}$. On the negative real axis, only the domain $0 < u \ll 1$ contributes significantly to the integral in the limit $x \rightarrow -\infty$. Hence, $\tau(u) \approx -\ln(u)$ and the function $h(x)$ is approximately

$$h(x) \approx - \int_0^\infty du e^{xu} (\ln u)^3 \approx - \frac{(\ln(-x))^3}{x}. \quad (\text{B2})$$

The last equality is obtained upon retaining the dominant term to the integral solely. Therefore, we can approximate $G(x)$ as

$$G(x) \approx -\bar{N}_0 \int_{\alpha_{\min}}^{\alpha_{\max}} d\alpha \phi(\alpha) \ln^3(-\alpha x) \sim -\bar{N}_0 \ln^3(-\langle \alpha \rangle x), \quad (\text{B3})$$

so that its derivative reads $G'(x) \approx -3\bar{N}_0 \ln^2(-\langle \alpha \rangle x)/x$. The condition $G'(x) = j$ leads to $x \approx -3\bar{N}_0/j$ for $j \ll 1$. Substituting this relation into the Legendre transform $F(j) = jx(j) - G[x(j)]$, we arrive at $F(j) \approx -\bar{N}_0 (\ln(j/j_c))^3$. We

also find $F''(j) \approx 3\bar{N}_0 (j \ln(j/j_c))^{-2}$. On inserting these expressions into Eq.(37), we obtain

$$P(j) \approx -\sqrt{\frac{3\bar{N}_0}{2\pi}} (j \ln(j/j_c))^{-1} e^{\bar{N}_0 \ln^3(j/j_c)}, \quad (\text{B4})$$

which leads to Eq.(38) after multiplication by j .

In the presence of source clustering, the behaviour of $\mathcal{G}(x) = G(x)\chi(x)$ in the limit $x \rightarrow -\infty$ strongly depends on the average clustering strength $(\bar{N}_e \bar{\xi}_2)(x)$, which is of positive sign on the whole negative real axis. For large cells, the integral over one of the position vectors drops out and we are left with

$$(\bar{N}_e \bar{\xi}_2)(x) \approx (-1)^\gamma \left(\frac{3\bar{N}_0 \tau_\xi^\gamma}{3 - \gamma} \right) x \int_{\alpha_{\min}}^{\alpha_{\max}} d\alpha \alpha \phi(\alpha) \times \int_0^\infty du e^{\alpha x u} (\ln u)^{3-\gamma} \quad (\text{B5})$$

in the limit $x \rightarrow -\infty$. We have assumed a powerlaw correlation with logarithmic slope γ . For $\gamma = 2$ close to the observed value, the integral over the variable u can be evaluated analytically :

$$\int_0^\infty du e^{\alpha x u} (\ln u)^{3-\gamma} \approx \frac{\ln(-\alpha x)}{\alpha x}. \quad (\text{B6})$$

Therefore, the average clustering strength scales according to

$$(\bar{N}_e \bar{\xi}_2)(x) \sim 3\bar{N}_0 \tau_\xi^2 \ln(-\langle \alpha \rangle x), \quad (\text{B7})$$

i.e. it diverges in the limit $x \rightarrow -\infty$. Since the void scaling function scales like $\chi \sim (\bar{N}_e \bar{\xi}_2)^{-1}$ for large average clustering strengths, we can approximate $\mathcal{G}(x)$ as

$$\mathcal{G}(x) \sim \frac{G(x)}{(\bar{N}_e \bar{\xi}_2)(x)} \sim -\frac{1}{3\tau_\xi^2} \ln^2(-\langle \alpha \rangle x). \quad (\text{B8})$$

Following the steps outlined above, we eventually find that the intensity distribution $P(j)$ scales as

$$P(j) \sim \exp \left[-\frac{1}{3\tau_\xi^2} \ln^2 \left(\frac{3\tau_\xi^2 j}{2\langle \alpha \rangle} \right) \right] \quad (\text{B9})$$

in the regime $j \ll j_c$. Note that this expression does not involve the mean number density \bar{n} of the sources.

B2 High-intensity tail

Consider the relation $F(j) + G(z) = jz$ which defines F and G as Legendre transforms. Let $f_n \equiv F^{(n)}(j_c)$ and $g_n \equiv G^{(n)}(z_c)$ denote derivatives of F and G at the critical point $(z_c, j_c) = (0, \langle j \rangle)$. Since g_2 is singular, the relation $g_2 f_2 = 1$ requires $f_2 \equiv 0$. In addition, $f_1 = z_c \equiv 0$ and $F(j_c) = j_c z_c - G(z_c) = 0$ since $G(z_c) = 0$. Therefore, a Taylor development of $F(j)$ and $F'(j)$ around j_c yields

$$F(j) = \frac{1}{6} f_3 (j - j_c)^3 + \dots \quad (\text{B10})$$

$$F'(j) = \frac{1}{2} f_3 (j - j_c)^2 + \dots \quad (\text{B11})$$

The bottom panel of Fig.3 demonstrates that f_3 must be a negative real number. On writing $F'(j) = z$, the second relation can be inverted to obtain $j(z)$, i.e.

$$j - j_c = -\sqrt{\frac{2}{f_3}} z^{1/2}. \quad (\text{B12})$$

The minus sign ensures that $j < j_c$ when $z < 0$. Hence, in the vicinity of $z_c = 0$, the function $G(z)$ reads

$$G(z) \equiv zj(z) - F[j(z)] \quad (\text{B13})$$

$$= zj_c - \frac{2}{3}\sqrt{\frac{2}{f_3}}z^{3/2} + \dots$$

which leads to Eq.(39). We then must expand $G(z)$ in the limit $z \rightarrow -\infty$.

The integral along the contour C is the sum of two contributions $I_1 + I_2$, where I_1 is the integral along the semi-circular contour of radius ϵ centered at $z = 0$ and

$$I_2 = \frac{1}{2\pi i} \left(\int_{-i\epsilon}^{-i\epsilon} dz + \int_{i\epsilon}^{i\epsilon} dz \right) e^{-jz+G(z)}. \quad (\text{B14})$$

Since $G(z^*) = G(z)^*$, the first integral is equal to minus the complex conjugate of the second. Furthermore, $I_1 \rightarrow 0$ in the limit $\epsilon \rightarrow 0$. Therefore,

$$P(j) = \frac{1}{\pi} \text{Im} \left\{ \int_{i\epsilon}^{i\epsilon} dz e^{-jz+G(z)} \right\}. \quad (\text{B15})$$

Substituting the series Eq.(39) into the argument of the exponential and taking the limit $\epsilon \rightarrow 0$, we have

$$P(j) \approx \frac{1}{\pi} \text{Im} \left\{ \int_0^\infty dx e^{-(j-j_c)x} \left[1 - \frac{2}{3}\sqrt{\frac{2}{f_3}}x^{3/2} + \dots \right] \right\}$$

$$= -\frac{1}{\pi} \text{Im} \left\{ \int_0^\infty dx e^{-(j-j_c)x} \frac{2}{3}\sqrt{\frac{2}{f_3}}x^{3/2} \right\}. \quad (\text{B16})$$

Performing the integral over x (which is proportional to $\Gamma(5/2)$), we arrive at Eq.(40).

The last step of the calculation is the evaluation of f_3 . Eqs. (32) and (B13) show that the function $h(z)$ must admit the series expansion

$$h(z) = 3 + c_{1/2}z^{1/2} + c_1z + \dots \quad (\text{B17})$$

in the vicinity of the critical point $z = z_c = 0$. A numerical evaluation of $(h(x)-3)x^{-1/2}$ in the limit $x \rightarrow 0$ yields $c_{1/2} = 2\sqrt{\pi}i$. The factor of i ensures that $h(x)$ is real on the negative real axis. Therefore,

$$G(z) = z\bar{N}_0 \int_{\alpha_{\min}}^{\alpha_{\max}} d\alpha \alpha \phi(\alpha) \left(3 + 2\sqrt{\pi}i\alpha^{1/2}z^{1/2} + \dots \right)$$

$$\approx zj_c + 2\sqrt{\pi}i\bar{N}_0 \langle \alpha^{3/2} \rangle z^{3/2}, \quad (\text{B18})$$

from which we easily read off the value of f_3 :

$$f_3 = -\frac{2}{9\pi\bar{N}_0^2 \langle \alpha^{3/2} \rangle^2} < 0. \quad (\text{B19})$$

Substituting this expression into Eq.(40) yields the desired expression Eq.(41).

In the presence of source clustering, we must consider the behaviour of the average clustering strength in the neighbourhood of $z = 0$. For a powerlaw correlation function, we have

$$(\bar{N}_e \bar{\xi}_2)(z) = - \left(\frac{3\bar{N}_0 \tau_\xi^\gamma}{3-\gamma} \right) z \int_{\alpha_{\min}}^{\alpha_{\max}} d\alpha \alpha \phi(\alpha)$$

$$\times \int_0^\infty d\tau \tau^{-\gamma} e^{z\alpha\tau^{-2}e^{-\tau}} e^{-\tau} (2+\tau) \quad (\text{B20})$$

in the limit of large cells. Unlike $h(z)$, the integral over τ

diverges in the limit $z \rightarrow 0$. This can be seen upon substituting the variable $w = \tau^{-2}e^{-\tau}$ as in Meiksin & White (2003). The τ -integral then becomes

$$\int_0^\infty dw \tau(w)^{3-\gamma} e^{z\alpha w} \approx \int_0^\infty dw w^{-(3-\gamma)/2} e^{-(-z\alpha)w}$$

$$= (-z\alpha)^{(1-\gamma)/2} \Gamma\left(\frac{\gamma-1}{2}\right). \quad (\text{B21})$$

The first equality follows from the assumption $\tau = w^{-1/2}$, which is a very good approximation at the small optical depths responsible for the divergence of the integral. For $\gamma \approx 2$, the integral diverges as $z^{-1/2}$. Therefore, applying the above Legendre transform to $(\bar{N}_e \bar{\xi}_2)(z)$ rather than $G(z)$ suggests that the average clustering strength admits the series expansion

$$(\bar{N}_e \bar{\xi}_2)(z) = c_{1/2}z^{1/2} + c_1z + c_{3/2}z^{3/2} + \dots \quad (\text{B22})$$

Eq.(B21) provides an estimate for the coefficient of the leading term,

$$c_{1/2} \approx -3\sqrt{\pi}i\tau_\xi^2 \bar{N}_0 \langle \alpha^{1/2} \rangle. \quad (\text{B23})$$

Here, the minus sign ensures that $\bar{N}_e \bar{\xi}_2 > 0$ when z is on the negative real axis. Using the fact that the void scaling function always behaves like $\chi(\bar{N}_e \bar{\xi}_2) \approx 1 - (1/2)\bar{N}_e \bar{\xi}_2$ for small clustering strength, we arrive at

$$\mathcal{G}(z) = G(z)\chi(z) \quad (\text{B24})$$

$$\approx zj_c + 2\sqrt{\pi}i\bar{N}_0 \langle \alpha^{3/2} \rangle \left(1 + \frac{9}{4}\tau_\xi^2 \bar{N}_0 \frac{\langle \sqrt{\alpha} \rangle \langle \alpha \rangle}{\langle \alpha^{3/2} \rangle} \right) z^{3/2}.$$

This implies that source clustering enhances the amplitude of the high-intensity tail $\propto j^{-5/2}$ by the factor given in the parenthesis. This enhancement is indeed observed in Fig.4, albeit with a ~ 6 times smaller amplitude.

REFERENCES

- Balian R., Schaeffer R., 1989, *Astron. Astrophys.*, 220, 1
 Bernardeau F., 1994, *Astron. Astrophys.*, 291, 697
 Bernardeau F., Kofman L., 1995, *Astrophys. J.*, 443, 479
 Bernardeau F., Pichon C., Codis S., 2013, *ArXiv e-prints*
 Bernardeau F., Schaeffer R., 1999, *Astron. Astrophys.*, 349, 697
 Berntsen J., Espelid T., Genz A., 1991, *ACM Transactions on Mathematical Software*, 17, 452
 Biagetti M., Chan K. C., Desjacques V., Paranjape A., 2014, *Mon. Not. R. Astron. Soc.*, 441, 1457
 Bolton J. S., Haehnelt M. G., Viel M., Carswell R. F., 2006, *Mon. Not. R. Astron. Soc.*, 366, 1378
 Bouchet F. R., Strauss M. A., Davis M., Fisher K. B., Yahil A., Huchra J. P., 1993, *Astrophys. J.*, 417, 36
 Boyle B. J., Griffiths R. E., Shanks T., Stewart G. C., Georgantopoulos I., 1993, *Mon. Not. R. Astron. Soc.*, 260, 49
 Boyle B. J., Shanks T., Peterson B. A., 1988, *Mon. Not. R. Astron. Soc.*, 235, 935
 Carruthers P., Shih C. C., 1983, *Physics Letters B*, 127, 242
 Colombi S., Bernardeau F., Bouchet F. R., Hernquist L., 1997, *Mon. Not. R. Astron. Soc.*, 287, 241
 Colombi S., Bouchet F. R., Schaeffer R., 1995, *Astrophys. J. Supp.*, 96, 401

- Conroy C., White M., 2013, *Astrophys. J.*, 762, 70
- Croom S. M., Smith R. J., Boyle B. J., Shanks T., Miller L., Outram P. J., Loaring N. S., 2004, *Mon. Not. R. Astron. Soc.*, 349, 1397
- Croton D. J., 2009, *Mon. Not. R. Astron. Soc.*, 394, 1109
- Croton D. J. et al., 2004, *Mon. Not. R. Astron. Soc.*, 352, 1232
- Davies F. B., Furlanetto S. R., 2014, *Mon. Not. R. Astron. Soc.*, 437, 1141
- Desjacques V., Nusser A., Sheth R. K., 2007, *Mon. Not. R. Astron. Soc.*, 374, 206
- Dixon K. L., Furlanetto S. R., 2009, *Astrophys. J.*, 706, 970
- Dixon K. L., Furlanetto S. R., Mesinger A., 2014, *Mon. Not. R. Astron. Soc.*, 440, 987
- Djorgovski S. G., Stern D., Mahabal A. A., Brunner R., 2003, *Astrophys. J.*, 596, 67
- Fall S. M., Geller M. J., Jones B. J. T., White S. D. M., 1976, *Astrophys. J. Lett.*, 205, L121
- Fardal M. A., Shull J. M., 1993, *Astrophys. J.*, 415, 524
- Faucher-Giguère C.-A., Lidz A., Zaldarriaga M., Hernquist L., 2009, *Astrophys. J.*, 703, 1416
- Font-Ribera A. et al., 2012, *JCAP*, 11, 59
- Francke H. et al., 2008, *Astrophys. J. Lett.*, 673, L13
- Fry J. N., 1985, *Astrophys. J.*, 289, 10
- Fry J. N., 1986, *Astrophys. J.*, 306, 358
- Fry J. N., Colombi S., 2013, *Mon. Not. R. Astron. Soc.*, 433, 581
- Fry J. N., Colombi S., Fosalba P., Balaraman A., Szapudi I., Teyssier R., 2011, *Mon. Not. R. Astron. Soc.*, 415, 153
- Furlanetto S. R., 2009, *Astrophys. J.*, 703, 702
- Furlanetto S. R., Oh S. P., 2008, *Astrophys. J.*, 681, 1
- Gaztanaga E., 1994, *Mon. Not. R. Astron. Soc.*, 268, 913
- Gleser L., Nusser A., Benson A. J., Ohno H., Sugiyama N., 2005, *Mon. Not. R. Astron. Soc.*, 361, 1399
- Gunn J. E., Gott, III J. R., 1972, *Astrophys. J.*, 176, 1
- Haiman Z., Hui L., 2001, *Astrophys. J.*, 547, 27
- Hamilton A. J. S., 1988, *Astrophys. J.*, 332, 67
- Hennawi J. F. et al., 2006, *Astron. J.*, 131, 1
- Hopkins P. F., Richards G. T., Hernquist L., 2007, *Astrophys. J.*, 654, 731
- Kaiser N., 1984, *Astrophys. J. Lett.*, 284, L9
- Kundić T., 1997, *Astrophys. J.*, 482, 631
- Lahav O., Saslaw W. C., 1992, *Astrophys. J.*, 396, 430
- Lepage G. P., 1978, *Journal of Computational Physics*, 27, 192
- Madau P., Haardt F., Rees M. J., 1999, *Astrophys. J.*, 514, 648
- Martini P., Weinberg D. H., 2001, *Astrophys. J.*, 547, 12
- Maselli A., Ferrara A., 2005, *Mon. Not. R. Astron. Soc.*, 364, 1429
- Meiksin A., Tittley E. R., 2012, *Mon. Not. R. Astron. Soc.*, 423, 7
- Meiksin A., White M., 2003, *Mon. Not. R. Astron. Soc.*, 342, 1205
- Mo H. J., White S. D. M., 1996, *Mon. Not. R. Astron. Soc.*, 282, 347
- Myers A. D., Richards G. T., Brunner R. J., Schneider D. P., Strand N. E., Hall P. B., Blomquist J. A., York D. G., 2008, *Astrophys. J.*, 678, 635
- Padmanabhan N., White M., Norberg P., Porciani C., 2009, *Mon. Not. R. Astron. Soc.*, 397, 1862
- Paschos P., Norman M. L., Bordner J. O., Harkness R., 2007, *ArXiv e-prints*
- Peebles P. J. E., 1980, *The large-scale structure of the universe*, Peebles, P. J. E., ed.
- Pei Y. C., 1995, *Astrophys. J.*, 438, 623
- Porciani C., Magliocchetti M., Norberg P., 2004, *Mon. Not. R. Astron. Soc.*, 355, 1010
- Prochaska J. X., Madau P., O’Meara J. M., Fumagalli M., 2014, *Mon. Not. R. Astron. Soc.*, 438, 476
- Ross A. J., Brunner R. J., Myers A. D., 2006, *Astrophys. J.*, 649, 48
- Schneider D. P. et al., 2000, *Astron. J.*, 120, 2183
- Shen Y. et al., 2007, *Astron. J.*, 133, 2222
- Sheth R. K., 1996, *Mon. Not. R. Astron. Soc.*, 278, 101
- Sheth R. K., 1998, *Mon. Not. R. Astron. Soc.*, 300, 1057
- Sokasian A., Abel T., Hernquist L., 2002, *Mon. Not. R. Astron. Soc.*, 332, 601
- Springel V. et al., 2005, *Nature (London)*, 435, 629
- Stephens A. W., Schneider D. P., Schmidt M., Gunn J. E., Weinberg D. H., 1997, *Astron. J.*, 114, 41
- Szapudi I., Colombi S., 1996, *Astrophys. J.*, 470, 131
- Szapudi I., Szalay A. S., 1993, *Astrophys. J.*, 408, 43
- Telfer R. C., Zheng W., Kriss G. A., Davidsen A. F., 2002, *Astrophys. J.*, 565, 773
- Tittley E. R., Meiksin A., 2007, *Mon. Not. R. Astron. Soc.*, 380, 1369
- Valageas P., 2002, *Astron. Astrophys.*, 382, 412
- Valageas P., Munshi D., 2004, *Mon. Not. R. Astron. Soc.*, 354, 1146
- White S. D. M., 1979, *Mon. Not. R. Astron. Soc.*, 186, 145
- Zuo L., 1992, *Mon. Not. R. Astron. Soc.*, 258, 36